GeoScienceWorld
Lithosphere
Volume 2024, Article ID lithosphere_2023_332, 28 pages
https://doi.org/10.2113/2024/lithosphere_2023_332

Lithosphere

Research Article

Complex Segment Linkage Along the Sevier Normal Fault, Southwestern Utah

Wanda J. Taylor[1], **Benjamin Surpless**[2] **and Ilsa M. Schiefelbein Kerscher**[3]

[1]*Department of Geoscience, University of Nevada Las Vegas, Las Vegas, 89154, USA*
[2]*Department of Earth and Environmental Geosciences, Trinity University, San Antonio, Texas, 78212, USA*
[3]*ExxonMobil, Spring, Texas, 77389, USA*

Correspondence should be addressed to Wanda J. Taylor; wanda.taylor@unlv.edu

Received 7 November 2023; Published 19 June 2024

Academic Editor: Elizabeth S. Petrie

Major normal fault systems are composed of segments that link as displacement accumulates, with linkage zone characteristics that reveal fault zone evolution. The steeply west-dipping Sevier fault zone in southwestern Utah, displays a complex fault network that developed between two long (>10 km), en echelon segments near the town of Orderville. Geologic map data and cross-sections of the transfer zone between the Mt. Carmel segment in the south and the Spencer Bench segment in the north reveal more than ten normal faults and four relay ramps displaying a range of geometries, including two relay ramps that display ramp-parallel folds. We suggest that transfer zone deformation was initially dominated by faults subparallel to the primary segments with later cross-faults that hard-linked these faults across most of the transfer zone. When the transfer zone was a soft-linked system, a displacement deficit likely existed relative to fault segments to the north and south. This early fault configuration would have reduced the efficiency of slip propagation associated with major earthquakes (>M7.0). In contrast, the present-day transfer zone, with a complex but hard-linked fault network, shows displacements that transition smoothly from the higher displacement (~800 m) southern segment to the lower displacement (~400 m) northern segment. That transition, combined with extensional strain within the zone, suggests that the Orderville fault network would be unlikely to impede propagation associated with future major earthquakes. The kinematic model of fault evolution presented here has implications for those investigating geothermal energy potential, groundwater flow, natural gas and oil reservoirs, mineral deposit formation, or seismic hazards.

1. Introduction

Over the past several decades, researchers have demonstrated that major normal fault systems are commonly segmented in map view and at depth, with segment linkage zone characteristics that can be used to reveal how long (10s–100s of km) fault zones evolve [1–10]. The interactions of fault segments at linkage zones perturb the local stress field, may permit slip transfer between fault segments, and can influence the formation of relay ramps, minor faults, and fracture networks [6, 11–13]. These fractures may promote fluid flow within a rock volume, so are important for evaluating oil and gas exploration, groundwater flow, and geothermal energy potential [13–17]. If heat flow is high enough, the intensely fractured damage zones associated with fault segment linkage [18] may be excellent targets for geothermal energy production [19–22]. Thus, a better understanding of fault network evolution and associated damage zone development will help future scientists more effectively target locations with high potential for geothermal energy production. In addition, because the entire length of long (from several km to over 100-km long) normal faults does not rupture during a single earthquake, linkage zones between segments play an important role in the evaluation of seismic hazard [23–28].

Many past studies focused on simple linkage zones, which improved our understanding of the mechanical interaction of separate fault segments [4, 12, 29–34]. For

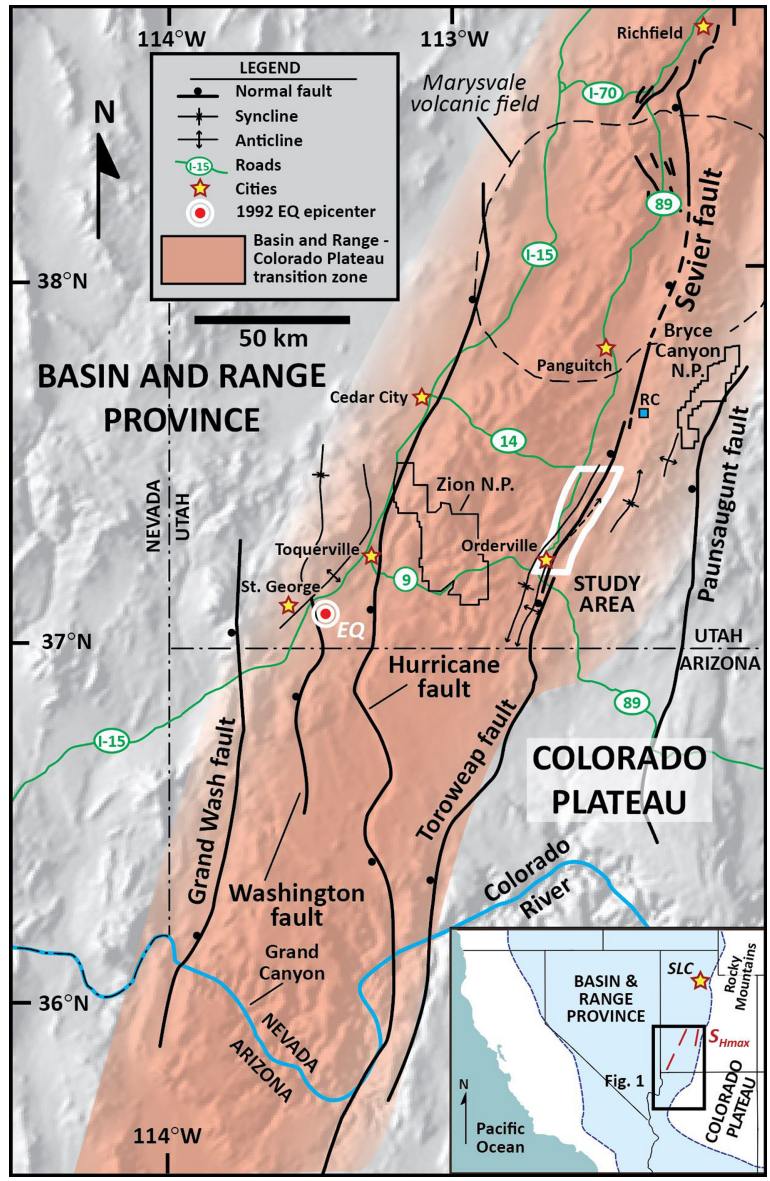

FIGURE 1: The Sevier fault zone study area within the Basin and Range-Colorado Plateau transition zone [see inset, with the location of Salt Lake City (SLC) indicated with a star]. The red lines on the inset figure are orientations of the maximum horizontal stress field (S_{Hmax}) as constrained by Lundstern and Zoback [101]. The Sevier-Toroweap fault, the Grand Wash fault, the Washington fault, the Hurricane fault, and the Paunsaugunt fault accommodate extension across the transition zone. Ball is on the hanging wall of faults. The epicenter of the 1992 M5.8 St. George earthquake is indicated by the red and white symbol, labeled "EQ" [97]. Approximate areal distribution of the Marysvale volcanic field is outlined by dashed lines. Blue box indicates the location of Red Canyon (RC), where Hecker [81] constrained slip rate along the Sevier fault. Study area boxed in white. Fold data are from Doelling et al. [45], Bowers [125], and Stewart and Taylor [65]. Digital shaded relief modified from Thelin and Pike [147]. Figure significantly modified from Reber et al. [35] and Surpless and McKeighan [148] with additional fault trace data from Hecker [81].

normal faults from meters to over 100-km long, fault growth by linkage of separate faults consists of propagation, local stress field interaction, possible formation of a relay ramp, and linkage [5, 6, 34]. Significant salients (geometric bends in the fault system that are convex toward the hanging wall) may also form at linkage zones [35, 36]. In most linkage zones, subparallel individual faults with displacement minima at their tips link, and the resulting synthetic fault segments (1) display parallel to sub-parallel strikes, (2) transfer slip from one fault to the other, and (3) exhibit displacement gradients with opposite polarities [12, 13, 33, 34, 37]. However, the linkage zone may not be simple; the three-dimensional geometric complexities of multipartite (involving multiple linkage zones) fault systems are just beginning to come to light [e.g., 37–41].

This range of complexities can be documented by detailed field investigations of complex linkage zones, such as those exposed along the central Sevier fault, southern Utah, which lies in the Basin and Range–Colorado Plateau transition zone (Figure 1). The segmented Sevier-Toroweap

normal fault (referred to as Sevier in Utah and Toroweap in Arizona) can be traced from the Grand Canyon in Arizona northward into the Miocene Marysvale volcanic field in Utah, where it loses its discrete character [42] (Figure 1). The Sevier fault likely initiated during the Miocene [35, 43] and can produce notable ground shaking and/or surface rupturing earthquakes based on fault length and presence of surface ruptures [43–47]. The central Sevier fault lies ~65 km (~40 mi) to the east of the Hurricane fault, near both Zion and Bryce Canyon National Parks (Figure 1), and is ideal to analyze fault linkage mechanisms because few preexisting structures complicate analysis and interpretation of the fault system, and multiple fault segments display a range of linkage zone geometries. The linkage zones between segments exposed there form the complexly deformed Orderville salient [35].

We use field and map data, including strike and dip of bedding, fractures and faults; kinematic measurements; and the spatial distribution of the faults and measurements, to document and analyze the well-exposed multipartite normal fault linkage zone within the Orderville salient. Our past [48, online Supplementary Material 1] and new geologic mapping and cross-section interpretations constrain geometries across the compound linkage zone that separates two primary Sevier fault segments.

We use these data to interpret that normal fault linkage was accommodated by a network of fault segments that controlled the formation of four relay ramps, which all transfer strain between initially en echelon primary fault segments. These geometries are far more complex than predicted in simple linkage models and provide data to more completely describe the evolution of the fault network. Our results have implications for the kinematic evolution of segmented normal fault systems worldwide and add detail to our understanding of how propagating earthquake rupture may be affected by segment boundaries.

2. Conceptual Background

2.1. Fault Segment Interactions and Relay Ramp Development. As synthetic normal faults within a system propagate laterally, they may begin to interact mechanically as the perturbed stress field at each fault's tip approaches the other fault (Figure 2) [12, 49]. Depending on the geometry of the interacting faults, these evolving stress fields may result in changes in the distribution of deformation in the linkage zone. The originally discrete faults may hard link and become segments of a single fault or may soft link via a zone of distributed strain, typically accommodated by a relay ramp. Because fault segment interactions control the evolution of the fault system as a whole and impact the propagation of earthquake rupture fronts [10, 50–53] and faults documented in this study are high-angle normal faults, we review the range of interactions possible between propagating, synthetic, high-angle normal faults.

The spacing and geometry of faults affect whether and how fault linkage will occur. If two faults are too widely spaced, local stress fields at fault tips will not interact and fault linkage will not occur, but fault dip and the subsurface distance between fault tip lines also affect the likelihood of linkage. For example, the steeper the fault dip, the closer in space the faults need to be in order to link at shallow depths; in contrast, faults with shallower dips can be spaced farther apart and still link at a shallow depth [12, 33]. However, fault spacing at the surface and at depth may differ because of changes in fault dip with depth, differences between the dip of each fault, and the shape of the fault tip lines, usually assumed to be elliptical [12, 33, 49]. For instance, Crider and Pollard [12] demonstrated that the first hard link between faults, and thus, the formation of segments on a single fault, is most likely to occur at the depth where fault tip lines are closest.

As en echelon normal faults propagate laterally in relatively close proximity, faults may link prior to or after their tips overlap across strike resulting in different linkage zone geometries (Figure 2). In some cases, faults curve toward each other and link with each other prior to overlap due to interacting stress fields (Figure 2(a)). If fault tips propagate past each other and overlap, a range of geometries is possible, including relatively simple fault propagation and connection (Figure 2(b)), fault capture (Figure 2(c)), or linkage by breakthrough faults (Figure 2(d)).

Linkage of overlapping faults typically includes an interaction phase during which a relay ramp forms due to stress field interactions between faults (Figure 2(e)) [12, 33]. Relay ramps connect the hanging wall of one fault segment to the footwall of another segment, effectively transferring strain and/or slip between the two segments, and may ultimately directly link the faults to form a single segmented fault [12, 13, 29, 34, 35, 37, 54–58]. A relay ramp typically transfers strain from the hanging wall of one fault to the footwall of the other fault by (1) tilting of the bedding within the ramp, forming a broad anticline at the top and syncline at the bottom, (2) vertical axis rotation, and (3) cutoff-parallel elongation without additional deformation within the relay ramp or the surrounding rocks (Figure 2(e)) [34]. Relay ramps commonly expand or propagate parallel to strike of the bounding faults. Hence, the relay ramp continues to deform to keep the hanging wall and footwall connected [34], but the interaction of the segment tips slows down the propagation rate of each fault [12, 59].

Because relay ramps help accommodate displacement gradients along fault segments, the geometry of the relay ramps can be related to displacement gradients of the bounding faults: a more geometrically complex relay ramp leads to a more complex displacement gradient [6, 29, 60]. In addition, greater displacement gradients along the bounding faults form steeper ramps [29, 58]. If ramp dip steepens beyond some critical value, relay ramps eventually are breached by linking faults, commonly at the base or top of the ramp (Figure 2(e)) [61], hard linking the fault segments by cross-faults and fracture networks [11, 34, 61]. As the two faults continue to slip, the faults may ultimately behave as a single fault [53, 56, 62].

2.1.1. Segment Boundaries and Earthquake Rupture. Researchers can identify segment boundaries based on surface observations of fault geometry and kinematic

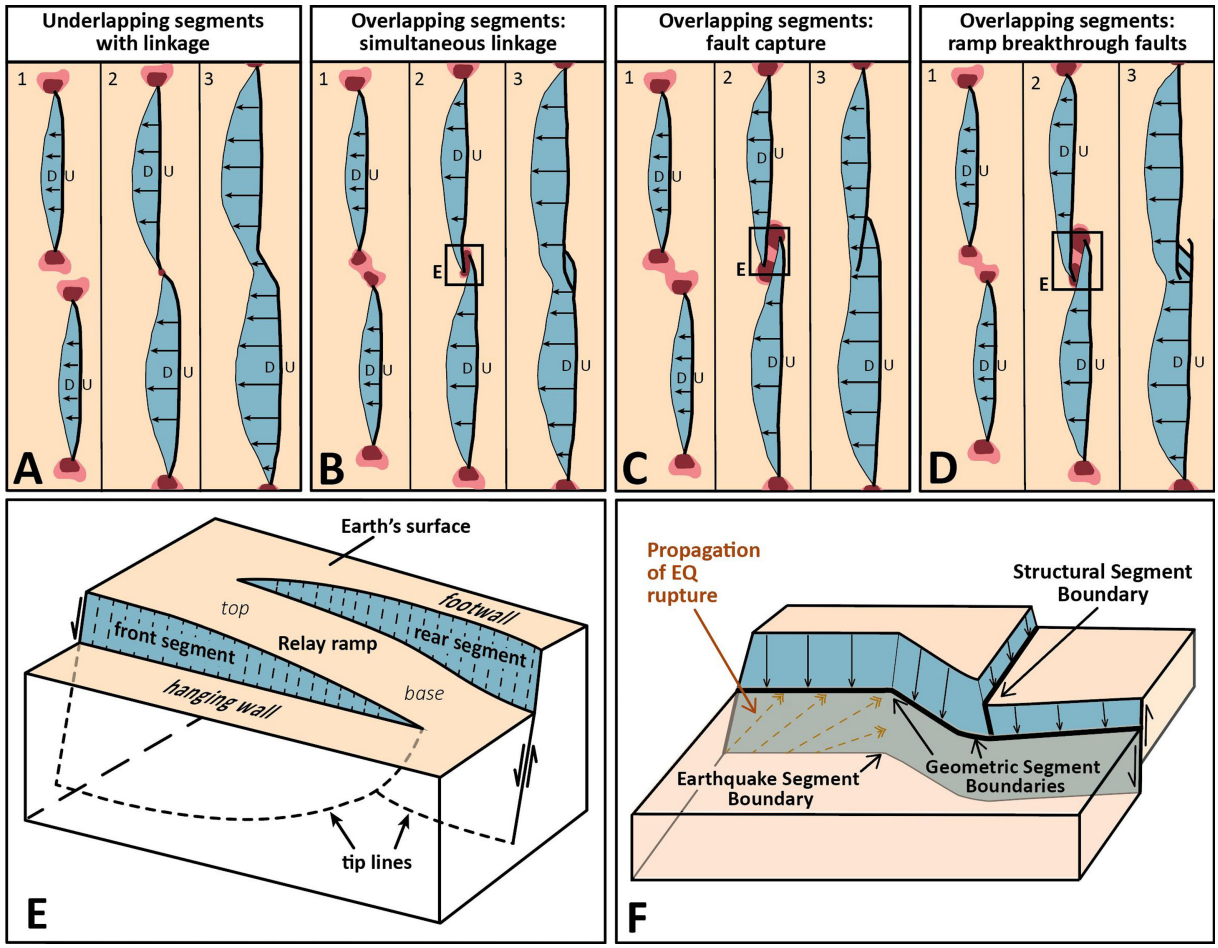

Figure 2: Diagrams displaying fault segment interactions, including stages of fault propagation and linkage, with stages 1-3 in chronological order (a–d), relay ramp development between en echelon normal faults (e), and examples of different segment boundary types (f). In all diagrams, the areas shaded blue with arrows represent fault displacement. (a) Linkage of underlapping fault segments. (b) Simultaneous linkage of overlapping fault segments. (c) Linkage by fault capture, where one segment takes over strain accommodation from the abandoned tip of the other segment. (d) Linkage by breakthrough faults, which usually form across a relay ramp. For diagrams A-D, the bold black lines are the footwall intersection lines of a normal fault. The dark- and light-red shading represents the approximate spatial distribution of elevated Coulomb shear stress based on computer modeling of en echelon normal faults by Crider and Pollard [12] and Crider [33]. The dark red areas have higher Coulomb shear stress values than the light red areas. Likely relay ramp locations are boxed (and labeled E). (e) Diagram illustrating a relay ramp developed between overlapping, en echelon normal faults. Schematic fault scarps display slip tapering to zero at the exposed fault tips, with semi-elliptical tip-lines in the subsurface. With increasing propagation and displacement, fault splays may hard link the segments, breaching the relay ramp at the top, base, or both (see stage 3 in diagram d). (f) Generalized diagram of both geometric and structural segment boundaries, both of which may control the location of an earthquake segment boundary. The blue shaded areas and thin arrows represent fault surfaces and offset, respectively. The bold lines represent normal faults, and the dashed red and orange arrows represent earthquake rupture or slip propagation direction. A segment boundary may be both a structural and a geometric boundary. In the diagram, a geometric boundary controls the position of an earthquake segment boundary, where rupture terminates. However, earthquakes may also initiate at geometric or structural boundaries. Diagrams (a–d) are modified from Reber et al. [35] and Taylor et al. [36]. Diagram (e) modified from Trudgill and Cartwright [56] and Crider and Pollard [12].

indicators as well as locations of scarps, footwall structures, and/or earthquake epicenters [24, 63–66]. However, many segment boundaries are not discrete, but are rather a broad, complexly faulted zone [67]. Importantly, both geometric and structural segment boundaries (Figure 2(f)) may control the position of rupture termination during earthquakes [63, 68, 69], so identifying and analyzing these types of segment boundaries along the central Sevier fault can aid in the assessment of both fault development and seismic hazard.

Geometric segments are recognized by changes in fault zone morphology (bends, step-overs, en echelon faults), changes in fault trace orientations and displacement, or gaps between fault segments in a fault zone (Figure 2(f)) [70, 71]. Geometric segment boundaries typically exhibit a dramatic change in strike that may shape a salient. These changes in strike commonly occur in zones of linkage. Structural segment boundaries occur at a preexisting structural discontinuity that impacts slip distribution and/or the fault tip stress field (Figure 2f) [69, 70].

Structural discontinuities are typically related to older structures that can be older faults or folds that strike at a high angle to the segmented fault (Figure 2(f)). A change in the geologic material crossed by the fault (e.g., changing from coherent rock to fault gouge back to coherent rock) may be a characteristic of a structural segment boundary [67, 71].

Some studies in seismology and fracture mechanics indicate that fault geometry can be important in the generation of earthquakes and rupture patterns [24, 69, 72, 73]. Indeed, studies along the nearby Hurricane fault (Figure 1) document recent earthquake ruptures that are limited to segments between geometric boundaries [74]. Researchers have suggested that geometric or structural segment boundaries along normal faults may not have a significant effect on earthquake ruptures during large (7.0+) magnitude earthquakes [4, 65]. However, smaller (e.g., M 3.0) earthquakes typically rupture only a single segment, so a geometric or structural segment boundary can serve as a barrier to rupture propagation [69, 70]. Zhang et al. [52] showed that the size of the segment boundary that can arrest earthquake rupture appears to scale proportionally with length and displacement during rupture.

An earthquake segment boundary is defined as a position along a fault where at least two earthquake ruptures have terminated, suggesting that the same boundary may therefore arrest future earthquake ruptures [63, 68]. Although it is possible to document earthquake segment boundaries using paleoseismological evaluation and assessment of fault data from historic earthquakes [52], we can also evaluate changes in total displacement across segment boundaries, with abrupt changes likely caused where a segment boundary serves as a consistent barrier to propagation over many earthquake cycles [75–78]. In the field, if multiple earthquake ruptures terminate at a given segment boundary, we might observe a zone that typically contains several fault splays and significantly fractured, crushed, and faulted rocks [67].

3. Structural Setting

The Basin and Range–Colorado Plateau transition zone varies in width from north to south in Utah and displays characteristics of each physiographic province. The zone displays a change in geologic characteristics from Basin and Range style extensional deformation to the less deformed, relatively stable Colorado Plateau [79]. In the north, the transitional region is narrower, with most extension accommodated along the Wasatch Front near Salt Lake City, Utah [79], while in southwestern Utah, the transition occurs across a much wider (~100 km) zone and includes multiple faults (Figure 1) [35, 79, 80]. Wannamaker et al. [79] suggest that the transition zone has structurally evolved since the onset of extension at 25–30 Ma.

The transition zone displays widely spaced Basin and Range-type normal faults (Figure 1) and is characterized by changes in crustal thickness across the transition between provinces. Crustal thickness in the Basin and Range Province varies from approximately 25–35 km, while the crust beneath much of the Colorado Plateau is more than 45 km thick [79]. At the latitude of the study area, the transition occurs between the approximate positions of the Hurricane and Paunsaugunt faults and displays crustal thickness values between 30 and 35 km thick [79, 81].

Multiple pre-Cenozoic tectonic events affected the southwestern Utah region, including, most notably, the Late Jurassic to mid-Cretaceous Sevier orogeny and the Late Cretaceous to Eocene Laramide orogeny [80, 82–87]. However, surface-breaking thrusts of the Sevier orogeny are thought to have extended only as far east as Cedar City (Figure 1) [88, 89]. Although evidence of the Laramide orogeny is present to the east and south of the Paunsaugunt fault (Figure 1) [42, 79], significant structures associated with the orogeny have not been documented near the study area. Thus, the study area has a relatively simple pre-Miocene structural history and is well suited to investigation of the evolution of Cenozoic extension within the transition zone.

On the west margin of the transition zone, the Hurricane fault is an active, segmented normal fault zone that strikes ~NNE [36, 65, 74, 90–92]. The most recent period of movement along the Hurricane fault probably initiated during the Miocene and continues today [36, 37, 74, 93]. Holocene fault scarps are exposed along the fault trace and several historic earthquakes have occurred along the Hurricane fault [90, 91, 94–98], with the 1992 M 5.8 St. George earthquake posited to have occurred along the fault based on the focal depth, epicenter location and aftershock solutions (Figure 1) [95–97].

Farther east, the Sevier-Toroweap fault strikes ~N30°E and dips 70–85°W along a trace length of ~350 km (220 mi) between the northern expression of faulting in Miocene volcanic rocks near Richfield and the southern tip south of the Grand Canyon, where it displaces Paleozoic rocks (Figure 1) [42, 45, 99]. The Sevier fault brittlely deforms nearly flat-lying to gently folded strata within the transition zone. Paleoseismic studies suggest that much of the Sevier fault in Utah has a vertical slip rate of <0.1 mm/yr and a recurrence interval between surface-faulting earthquakes of ≥~30 kyr since 12–15 Ma [43]. The central Sevier fault has not been observed cutting Holocene sediments, but Jackson [100] and Hecker [81] suggested that evidence for recent activity may be obscured by active colluvial slopes and thick vegetation. The Sevier fault displaces Quaternary basalt and sediments, however, which suggests at least Quaternary activity [96]. Quaternary deformation is common in the region. Hundreds of M<5 and a few M5–7 earthquakes have been recorded or documented since 1850 in southwestern Utah. The seismic record includes many small earthquakes within 5 km of the Sevier fault [94, 95], which suggests that this fault may be active. Generally, the NNE-striking strands of the Sevier fault are favorably oriented to host an earthquake because the regional stress field has a NNE-SSW oriented maximum horizontal stress (Figure 1) [101].

The Paunsaugunt fault is the easternmost ~NNE-striking normal fault in the transition zone. The fault trace extends ~65 km (~40 mi) [42]. The Paunsaugunt fault is thought to be the oldest of the three faults because the hanging

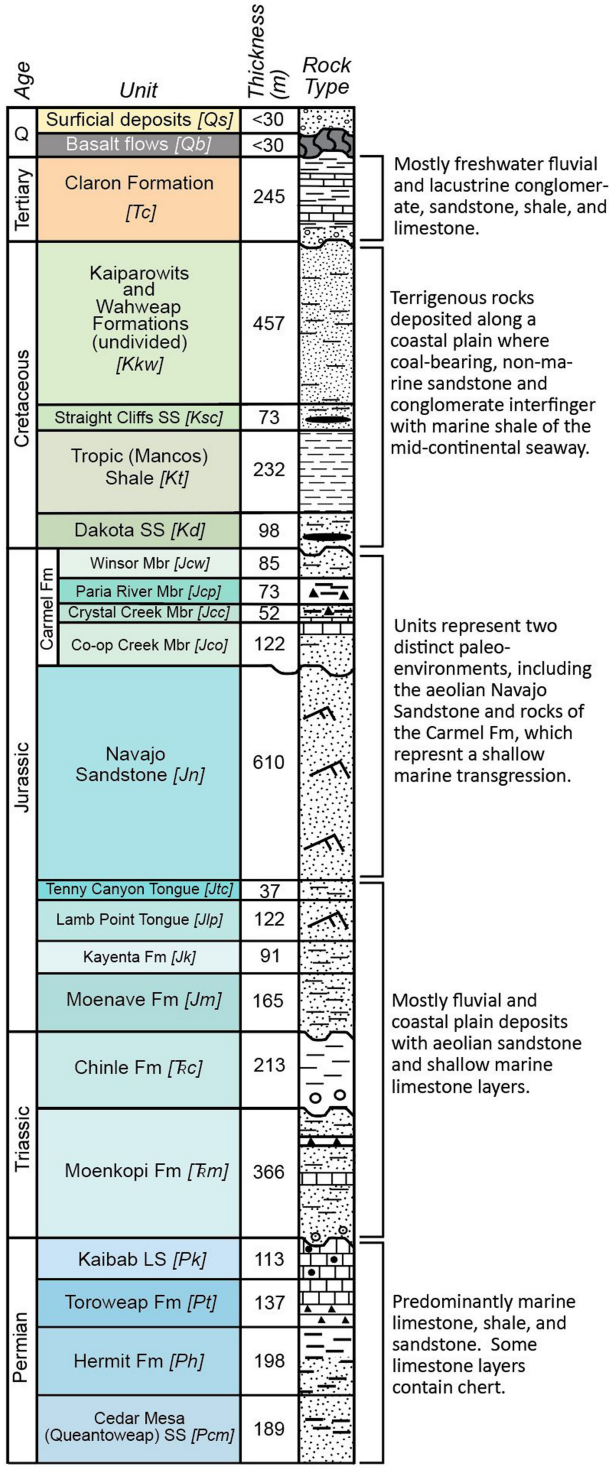

FIGURE 3: This stratigraphic column represents units exposed on the surface as well as units known in the subsurface of the study area. Standard symbols are used for rock types; wavy bands are used for volcanic flows, black ovals are used for coal, triangles are used for gypsum, open angles with lines represent cross-beds, and filled circles are used for chert. Data from Gregory [99], Cashion [149], Hintze [88, 108], Rowley et al. [110], Marzolf [109], Stokes [106], Doelling et al. [45], and Goldstrand [112].

wall is topographically higher than the footwall, an unusual feature possibly caused by a more resistant lithologic unit capping the hanging wall than the footwall. Such topographic reversal takes significant time to form, supporting the suggestion that the Paunsaugunt fault has not ruptured in the Quaternary [102]. The balanced rocks (hoodoos) of the Tertiary Claron Formation in Bryce Canyon National Park (Figure 1) also may suggest a lack of large recent seismic events [42, 103, 104].

4. Stratigraphy

The stratigraphy exposed along the central Sevier fault consists of a thick succession of late Triassic to Cretaceous carbonate and siliciclastic rocks, which are unconformably overlain by Cenozoic volcanic and sedimentary units (Figure 3). The exposed Mesozoic section is approximately 2300 m (7546 ft) thick, gently folded, and generally dips to the northwest and northeast [45, 88, 99, 105–109]. The many thin, well-defined Mesozoic units (Figure 3) are ideal for documenting small fault displacements and allowing relatively small uncertainties in the calculations of the stratigraphic throw across faults, which is the primary use of stratigraphy in this study. The depositional environments of the exposed Mesozoic units range from shallow marine to fluvial and coastal plain deposits with aeolian sandstone [e.g., 45, 99, 109]. The Triassic units were deposited in mostly fluvial and coastal plain environments with aeolian sandstone and shallow marine limestone layers. Jurassic units represent two different paleo-environments: (1) aeolian deposits of the Navajo Sandstone and (2) shallow marine transgression rocks of the Carmel Formation [e.g., 45, 109]. Cretaceous units are composed of terrigenous rocks that were deposited along a coastal plain where coal-bearing units, non-marine sandstone, and conglomerate interfinger with marine shale of the mid-continental/western interior seaway [e.g., 88, 106, 108]. During Jurassic and Cretaceous, a highland created by the Jurassic to Cretaceous Sevier Orogeny lay to the west and provided much of the clastic materials [80, 87–89]. A detailed description of the lithologic units in and near the central Sevier fault is presented in Schiefelbein [48, online Supplementary Material 1]. Units and thicknesses that are Triassic and older on cross-sections, but not exposed in the map area, are from Hintze [88, 108], Marzolf [109], and Doelling et al. [45] (Figure 3).

Tertiary and Quaternary volcanic and sedimentary units unconformably overlie the Mesozoic succession (Figure 3). The Cenozoic section is approximately 300 m (984 ft) thick (Figure 3) [45, 88, 99, 105–108]. The Tertiary succession consists of the Claron Formation, a freshwater unit with mostly fluvial and lacustrine conglomerate, sandstone, shale, and limestone [45, 106, 110–112]. The unconformity at its base in the area is slightly angular and sub-planar.

Late Cenozoic basalt is common in the transition zone and erupted from a series of small-volume late Miocene to Quaternary mafic centers [107, 113, 114]. Quaternary flows (Qb) crop out in the mapped area (Figure 4) and where

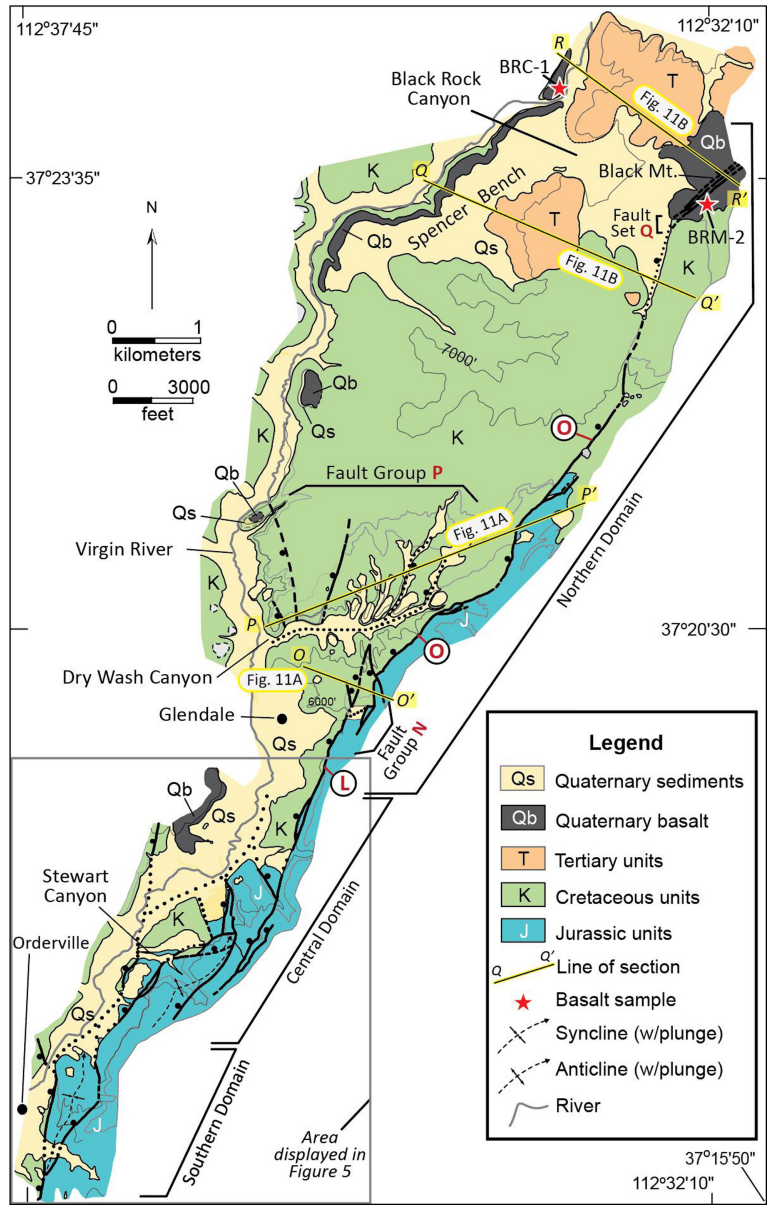

FIGURE 4: Simplified geologic map of the study area. Geographic locations and sample collection sites are indicated. The bold lines are faults (dashed where inferred, dotted where obscured by alluvium). The Virgin River is shown by a bold gray line. Basalt sample sites indicated by red stars. Area outlined by the gray box is displayed in Figure 5. See Figure 11 for cross-sections O-O′, P-P′, Q-Q′, and R-R′. The towns of Orderville and Glendale are indicated by black circles.

exposed along the Sevier fault are offset or tilted by the Sevier fault (Fault Set Q; Figure 4).

Quaternary sedimentary units (Qs on Figures 3 and 4) include fluvial deposits, spring deposits, stream terraces, slope failures, colluvium, sinter-type spring deposits, and alluvium that unconformably overlie units ranging from Jurassic through the early Tertiary. The unconformity at the base is slightly angular and has irregular paleorelief; the distribution and thickness (<30 m, Figure 3) of these deposits are limited. Most Quaternary sediments are younger than the ~570 ka basalt flows (dated in this study) because the deposits contain basalt clasts and grains [48]. However, the ~570 ka basalt flows (Qb) unconformably overlie Quaternary conglomerates ~8 km (~5 mi) northeast of Glendale and ~1 km (0.6 mi) southwest of Glendale. No growth strata were observed.

5. Methods

We previously mapped [48, online Supplementary Material 1] and collected new geologic map data at the 1:12,000 scale across approximately 30 km^2 (~12 mi^2) of Kane County, southwestern Utah, using standard geologic mapping techniques. We used a topographic base derived from the Orderville, Glendale, and Long Valley 7.5′ U.S.G.S. quadrangles, and we used color aerial photographs and satellite imagery to aid field-based mapping. However, all mapping presented here is based on direct field observa-

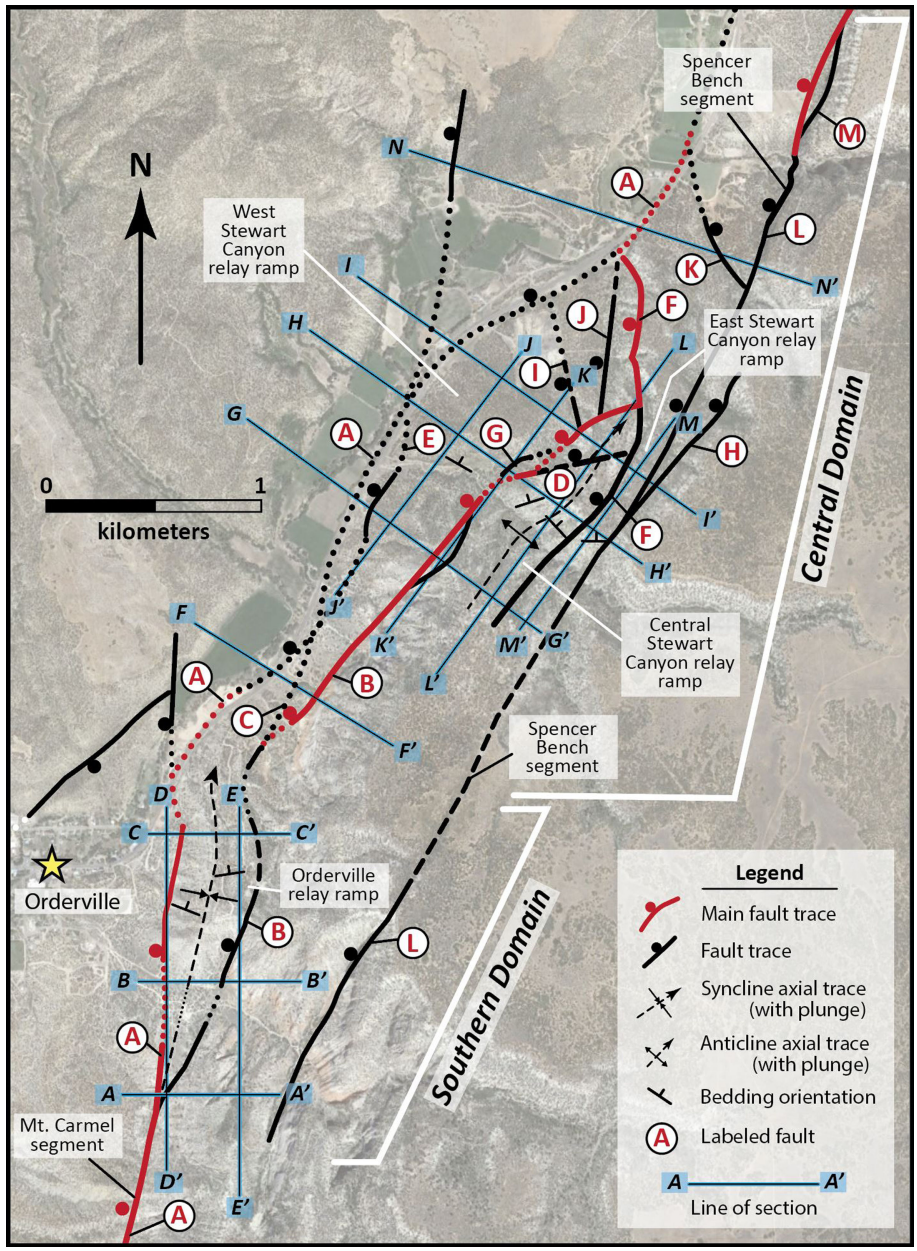

FIGURE 5: Structure map of the fault network within the Southern and Central Domains of the central Sevier fault zone study area, displaying lines of section for all cross-sections in the Southern and Central Domains. All faults important for this study are labeled with red letters. Thick red lines are the main strands of the Sevier fault zone, which display the greatest throw of the faults at that latitude. Ball symbols are on the hanging wall of normal faults. Lines of section A–A′ through N–N′ are displayed as blue lines. The town of Orderville is displayed as a yellow star. See Figure 4 for the location of this figure within the study area.

tions. A map of most data can be downloaded from https://digitalscholarship.unlv.edu/rtds/1393/ [48] and found in the online Supplementary Material 1. New mapping by the authors has constrained the southern extent of the Spencer Bench segment, which extends farther south than the originally mapped segment [48]. All stereographic projections and analyses were performed using the computer software GEOrient.

We identified faults based on the displacement of stratigraphic units as well as the exposure of fault breccia, gouge, and localized mineralization associated with hydrothermal alteration. Because of the limited number of kinematic indicators, we did not determine the exact net-slip direction for faults. Because the dip of most faults in this study is greater than 65° and the units displaced by faulting dip shallowly, we use fault stratigraphic throw to quantify slip. Throughout this document, we use "throw" to indicate "stratigraphic throw."

We constructed retrodeformable cross-sections from structural and stratigraphic data and geometries. Most cross-sections were drawn approximately perpendicular to the strike of the faults to analyze along-strike variations

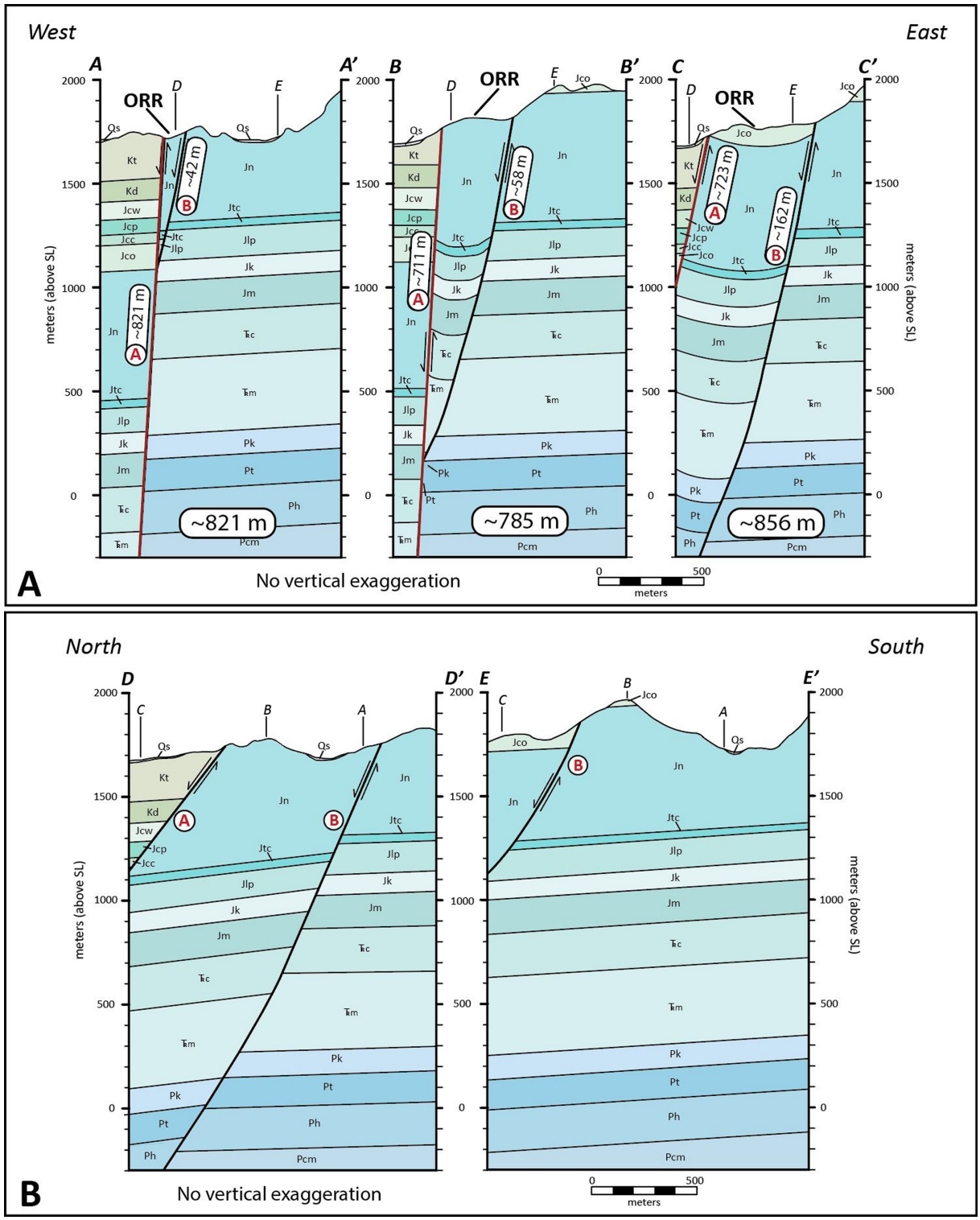

FIGURE 6: Cross-sections from the Southern Domain with throw values shown in white boxes (fault stratigraphic throw values displayed at base of each cross-section). Red text in white circles indicates named faults (Figure 5). (a) Cross-sections A–A′, B–B′, and C–C′, constructed along E-W lines of section (Figure 5). (b) Cross-sections D–D′ and E-E′, constructed along N-S lines of section (Figure 5). Vertical lines at the top of each cross-section are lines of intersection with other cross-sections. See Figure 3 for the complete names of all stratigraphic unit abbreviations. The red fault is the main trace of the Sevier fault system at that latitude. Cross-sections A-A′ through E-E′ were used to construct the fence diagram displayed in Figure 7. The Orderville relay ramp (ORR) is labeled. All cross-sections constructed with no vertical exaggeration.

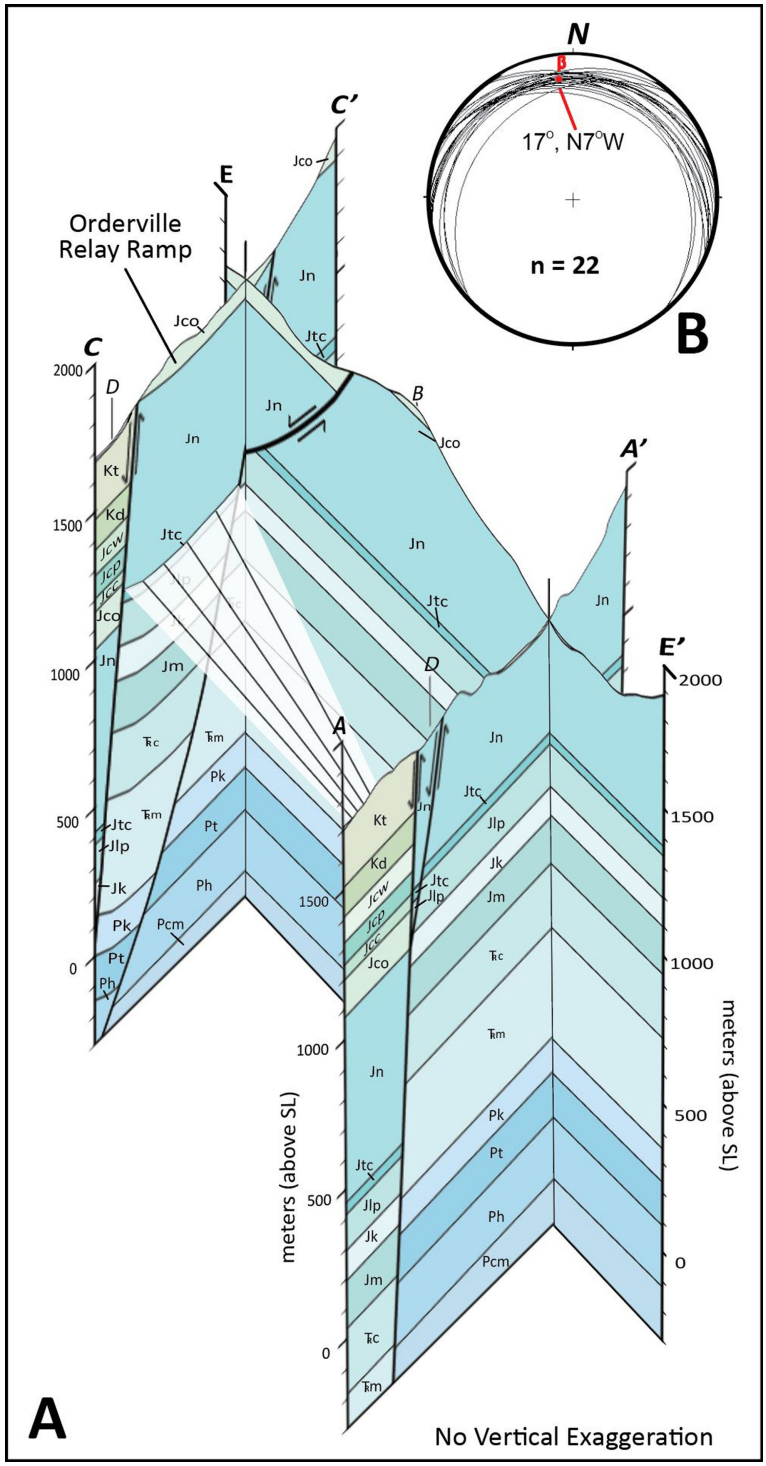

FIGURE 7: (a) Southern Domain fence diagram focused on the fault-parallel syncline within the Orderville relay ramp. Strata outside the relay ramp are nearly flat lying. Bold lines represent normal faults, and white shading represents the relay ramp syncline with lines representing structural contours. The stratigraphy is displayed in Figure 3. Cross-sections in Figure 6 were used to constrain the shape of the anticline, but cross-sections B–B′, and D–D′ are not displayed in order to better reveal syncline shape. (b) Equal-area stereonet displaying bedding in the syncline and the N-trending, shallowly plunging syncline axis (beta plot) within the Orderville relay ramp.

of displacement along major segments, in splay zones, and along isolated strands of the fault network. Fault attitudes were calculated by three-point problems and/or structure contours because no faults in the study area yielded a

measurable surface. Subsurface fault geometries are based on the surface data and our ability to effectively retrodeform each cross-section.

We used standard cross-section retrodeformation techniques for all presented cross-sections [115–122]. We constructed cross-sections under the assumptions that plane strain occurred, and rock volume and bed thicknesses remained constant. In all cross-sections, bed lengths balance and no loss of area occurred, within a standard uncertainty of 5–10%. We assume constant fault displacement with depth because we cannot directly constrain subsurface fault geometries. We also assume simple fault geometries at depth because we have no evidence to suggest that the dip angles of the faults change with depth or that flower structures exist in the subsurface. We attempted to remain true to the surface data while still considering how different fault segments most likely interact at depth. Subsurface unit thicknesses are based on (1) the calculated thickness from the map pattern of exposed units in the study area and (2) the published thicknesses of subsurface units (Figure 3) [10, 45, 88, 108]. We tested and modified completed cross-sections based on results from 3D computer model construction using the MOVE 2022 core application [123].

We also collected and dated two basalt samples to provide timing constraints on deformation (see online Supplemental Material for $^{40}Ar/^{39}Ar$ data). $^{40}Ar/^{39}Ar$ dating was performed on basalt samples at the Nevada Isotope Geochronology Laboratory (NIGL) at the University of Nevada Las Vegas. Relevant $^{40}Ar/^{39}Ar$ dating methods are described in the online Supplementary Material 2.

6. Structural Data And Results

Data presented here reveal four relay ramps and a fault salient that accommodate extension along the central Sevier fault zone. We subdivide the central Sevier fault into the Southern domain, which includes the Orderville relay ramp; the Central domain, which includes the Stewart Canyon overlap zone; and the Northern domain (Figure 4). We use the term "main strand" to indicate the fault with the greatest displacement at a given latitude based on cross-section interpretations; thus, the fault that is the main strand changes along strike. The strikes of the main strands vary significantly, from N5°E to N80°E, a 75° variation about the general ~N30°E strike. This range of strikes reflects along-strike curves in the faults. Importantly, previous researchers [40] documented long-wavelength folds across the region, and we consider these tilts when reconstructing extension in cross-section.

6.1. Southern Domain. The Southern Domain extends from near the southern boundary of the map area to ~1 km (~0.6 mi) north of the community of Orderville (Figures 4 and 5), where Davis [42] made preliminary structural and stratigraphic observations of the Orderville relay ramp. Near the southernmost extent of the Southern Domain, where the Mt. Carmel segment (Fault A) splits into two splays (Faults A and B), the total throw across the fault zone is ~821 m (2695 ft.) (section A–A′; Figure 6). The Orderville relay ramp is bound by Faults A and B. Fault A, the main strand of the Sevier fault in the Southern Domain, generally strikes N10°E and dips 76°W but the strike changes from ~N-S in the south to NE in the north (Figure 5). Fault A juxtaposes the Cretaceous Tropic Shale (Kt) against Jurassic Navajo (Jn) Sandstone (sections A–A′, B–B′, C–C′; Figure 6). Fault B dips 79°W and generally strikes N40°E but has sections that alternate between N and NE strikes (Figure 5). To the north, this fault juxtaposes the Jurassic Co-op Creek Member of the Carmel Formation against the Jurassic Navajo modifying Sandstone (section C–C′; Figure 6).

Fault A, the main strand, accommodates most of the total throw across the Sevier fault at this latitude, but Fault B accommodates an increasing portion of throw across the system northward, increasing from ~42 m (~130 ft.) at the latitude of section A–A′ to ~162 m (~531 ft.) at the latitude of cross-section C–C′ (Figure 6). These faults are linked in map view (Figure 5), and bedding dip differences across the faults as well as cross-section construction and retrodeformation indicate that these faults connect in the subsurface (Figures 6 and 7).

Within the Orderville relay ramp, map patterns, cross-sections, and stereograph analysis show a plunging syncline with an axis oriented 17°, N7°W (Figures 5–7). The syncline is a gentle, subhorizonal, upright fold. However, to the west of Fault A and to the east of Fault B, the strata are generally flat lying to gently west dipping (Figures 6 and 7). The relay ramp terminates at its base by intersection of Faults A and B, at least to the south. We suggest that depth to the base increases from south, at a depth of ~670 m (2200 ft) (section A–A′), to north, where faults intersect at a depth of ~2135 m (7000 ft) (section C–C′; Figures 6 and 7).

6.2. Central Domain. The Central Domain extends from ~2 km (~1.3 mi) northeast of Orderville to ~1 km (~0.67 mi) south of Glendale (Figures 4 and 5). We refer to the southern part of the Central Domain as the Stewart Canyon overlap zone, where several faults overlap in map view and help accommodate extension in the vicinity of Stewart Canyon (Figure 5). The total throw across the faults in this domain ranges from ~687 to ~823 m (2250 and 2700 ft.) (Figure 8).

Cross-section F–F′, at the southernmost extent of the Central domain, displays ~780 m (2560 ft.) total throw across the Sevier system (Figure 8), a value lower than the throw values of the Southern Domain. At this latitude, Fault B displays the greatest throw (~431 m; 1410 ft.), suggesting that it has become the main trace of the Sevier fault zone at this latitude (Figures 5 and 8). We project Fault A so that it connects with Fault B at a depth of 1280 m (4200 ft) (Figure 8), and we project Fault C to connect at depth with Fault A at a depth of 960 m (3150 ft) (Figure 8).

The strikes of the main strand of the Sevier fault within the Stewart Canyon overlap zone change northward, from N35°E to N65°E to N–S (Figure 5), with dips that vary from 76 to 84° W or NW. In this region, most of Fault A is buried by Quaternary alluvium (Figure 5), but we infer

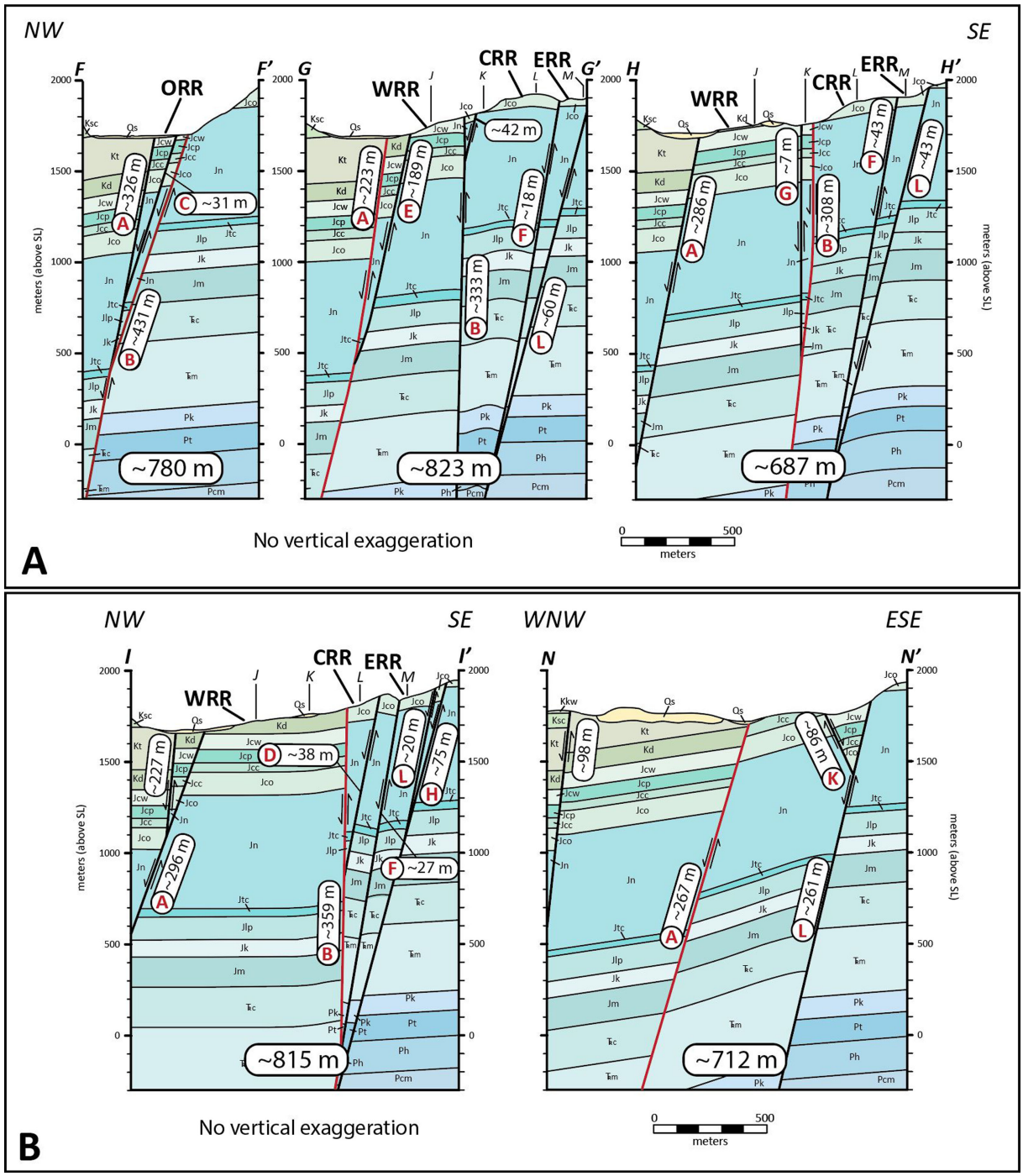

FIGURE 8: Cross-sections F–F′ through I–I′ and N–N′ from the Central Domain of the Sevier fault zone study area (see Figure 5 for lines of section). Total fault stratigraphic throw values are displayed at base of each cross-section. Red text in white circles indicates named faults (Figure 5). Vertical lines at the top of each cross-section are lines of intersection with other cross-sections. See Figure 3 for the complete names of all stratigraphic unit abbreviations. (a) Cross-sections F–F′, G–G′, and H–H′ constructed along NW-SE lines of section, approximately perpendicular to fault strike (Figure 5). Section F–F′ displays the fault geometries where deformation is limited to a narrow fault-perpendicular width relative to the complexly faulted zones to the north and south. (b) Cross-sections I–I′ and N–N′, constructed approximately perpendicular to the strike of the Sevier fault zone (Figure 5). Cross-sections G–G′ and I–I′ were used to construct the Central Domain fence diagram displayed in Figure 10. Relay ramp abbreviations: ORR = Orderville relay ramp; WRR = West Stewart Canyon relay ramp; CRR = Central Stewart Canyon Relay Ramp; and ERR = East Stewart Canyon relay ramp. All cross-sections constructed with no vertical exaggeration.

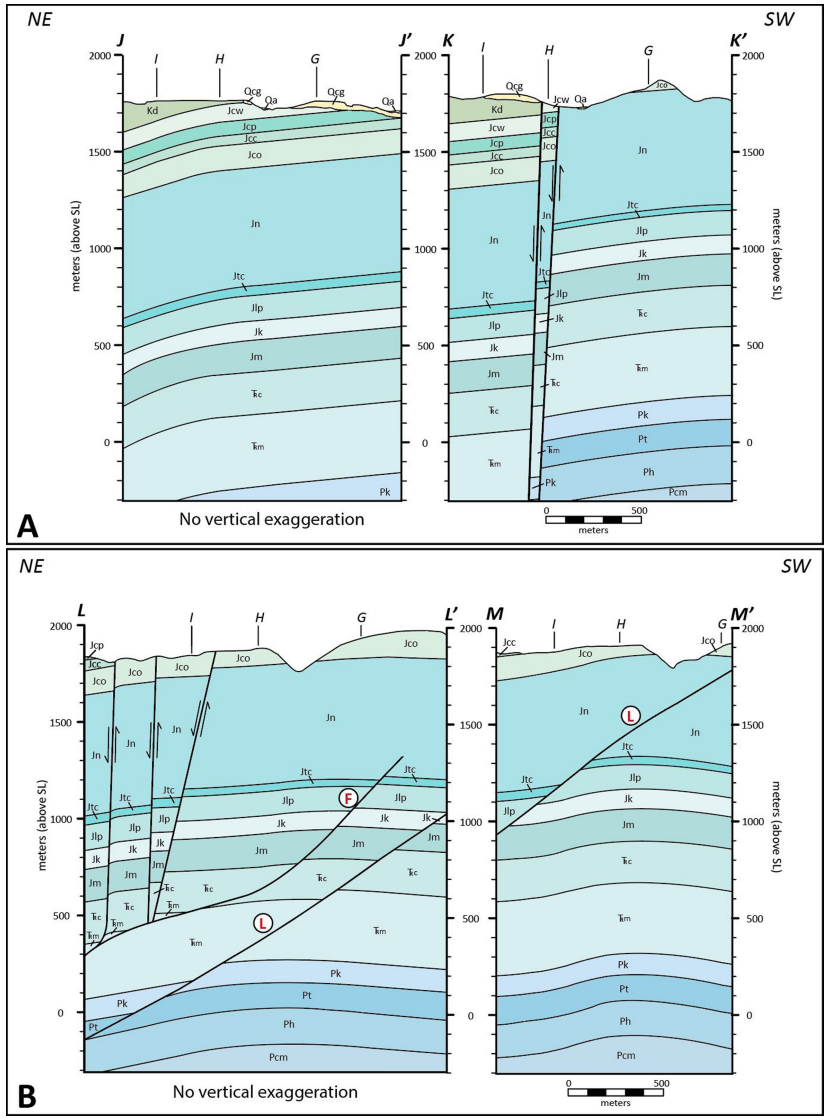

Figure 9: Cross-sections J–J′ through M–M′ are from the Central Domain of the Sevier fault zone study area. Cross-section M–M′ was used to construct part of the Central Domain fence diagram displayed in Figure 10. Vertical lines at the top of each cross-section are lines of intersection with other cross-sections. (a) Cross-sections J–J′, and K–K′ constructed along NE-SW lines of section (Figure 5). (b) Cross-sections L–L′ and M–M′, constructed along NE–SW lines of section (Figure 5). Note that Faults F and L intersect lines of section L–L′ and M–M′ at low angles, so cross-sections display dips significantly shallower than true dips. See Figure 3 for the complete names of all stratigraphic unit abbreviations. All cross-sections constructed with no vertical exaggeration.

the presence of the fault at these locations based on the differences in the units exposed across strike and retrodeformable cross-sections (Figures 8 and 9).

The overlap zone adjacent to Stewart Canyon contains 11 fault strands with a range of orientations, striking from NNW to ENE (Figure 5) with dips from 69° to 84° to the N and W. Most of these faults connect at the surface (Figure 5), with the exception for the easternmost two faults (Faults L and H), which do not connect with the western faults in map view. Abutting relationships help us delineate different fault populations and provide constraints on relative timing [38, 40], with Fault F abutting Fault A, and Faults D and G abutting Fault F (Figure 5). Faults I and J terminate where they abut Fault A in the north and Fault B in the south (Figure 5). Most remaining faults across the overlap zone display low angles relative to the faults they intersect (e.g., Faults E and H).

Our cross-section construction and restoration suggest that all faults within the Stewart Canyon overlap zone, including Faults L and H, connect in the subsurface, with strands that project down-dip and connect at depth (Figure 8; section I–I′). Three relay ramps occur within the Stewart Canyon overlap zone: the West, Central, and East Stewart Canyon relay ramps (Figures 5, 8 and 10). The ramps have steeply dipping bounding faults that either connect or apparently connect at depth.

The West Stewart Canyon relay ramp is an apparent breached ramp with both base and top breaches (Figure 2(e)). The bounding faults appear to connect at the surface on both the north (Fault F) and south (Fault C), but

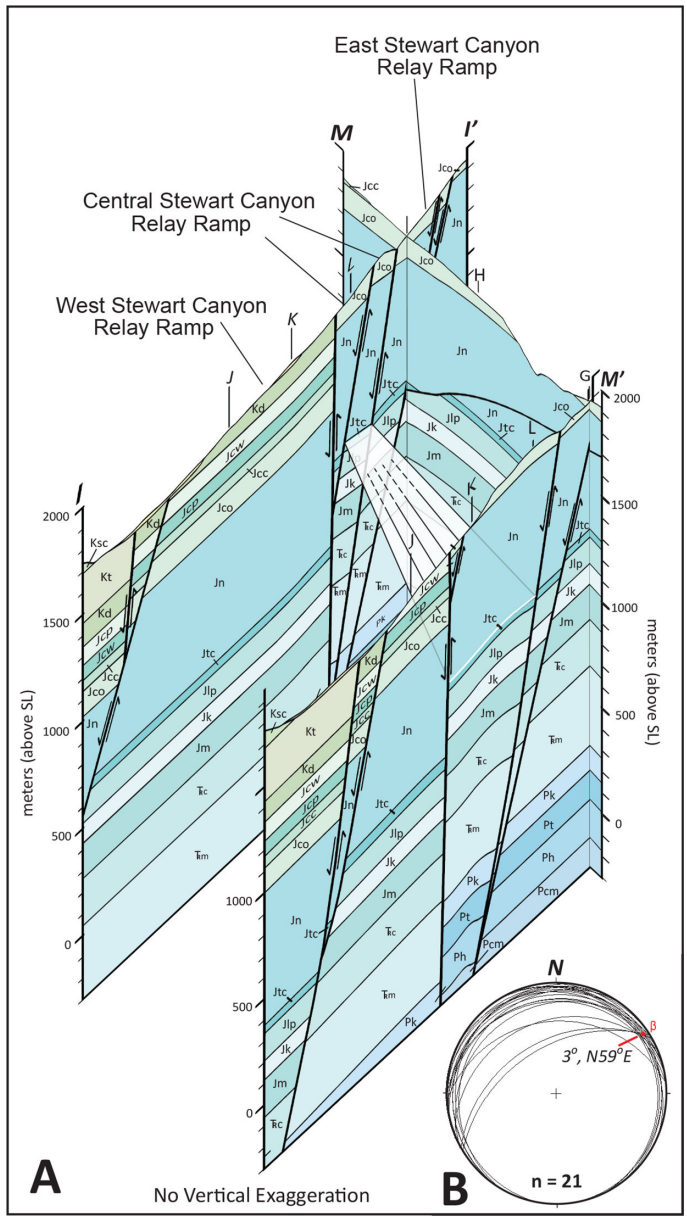

FIGURE 10: (a) Central Domain fence diagram, focused on the fault parallel anticline within the Central Stuart Canyon relay ramp. Strata outside the relay ramp are nearly flat lying, but strata within the ramp form a fault-parallel anticline. Note that cross-faults breach the northeastern section of the relay ramp (Figure 5). Bold lines represent normal faults, and white shading represents relay ramp anticline with axis-parallel lines representing structural contours. The stratigraphy is displayed in Figure 3. Cross-sections in Figures 8 and 9 were used to constrain the shape of the anticline, but cross-sections H–H′, J–J′, K–K′, and L–L′ were removed to better reveal anticline shape. (b) Equal-area stereonet displaying bedding in the anticline and the NE-trending, shallowly plunging anticline axis (beta plot).

western bounding fault (Fault A or E) is mostly buried by Quaternary alluvium (Figure 5). Although our cross-section projections of bounding faults do not show convergence with increasing depth, the faults may connect in the subsurface. Two cross-faults (I and J) also cut the base of the ramp and abut the bounding faults (Figures 5, 8 and 10). We documented a NE-dipping ramp monocline (Figure 5 and section J-J′ in Figure 9) and no other folds, but not all of the relay ramp is exposed.

The Central Stewart Canyon relay ramp and the anticline within it are bound by two steeply dipping, planar faults (Figures 5, 8 and 10). These faults project down-dip to connect at an estimated depth of ~1890 m (6200 ft) on the north (section I–I′) and a depth of ~2590 m (8500 ft) on the south (section G-G′; Figure 8). The bounding faults connect at the surface at the structurally lowest point of the ramp (NE of the axial plunge arrow in Figure 5), indicating that the ramp is base breached (Figure 2(e)). A NE-striking

cross-fault (Fault D) cuts the relay ramp, displacing the fold axis, and abuts the ramp-bounding faults in map view (Figure 5). This planar cross-fault appears to abut the east bounding fault at the surface as well as at depth, projected to occur at 930 m (3050 ft) depth (section I–I′; Figures 8 and 10). Within the Central Stewart Canyon relay ramp, map patterns and cross-sections show a gentle, sub-horizontal, upright, northeast-plunging anticline-oriented 3°, N59°E (Figure 10). East and west of the Stewart Canyon overlap zone, the strata are gently west dipping (3°, 7°) (Figure 8), indicating that the anticline is restricted to the ramp.

The East Stewart Canyon relay ramp lies between the same fault that forms the eastern boundary of the Central Stewart Canyon relay ramp (Fault F) and subparallel, steeply northwest-dipping Fault L (Figure 5). The bounding faults do not link in map view; however, they may link at depth (Figures 8 and 10). The north-dipping ramp monocline displays shallowly north-dipping bedding attitudes (11°, 16°) (Figure 5).

Farther north, at the latitude of cross-section N–N′, the main strand of the Sevier fault, Fault A, only displays 267 m (876 ft) of throw where it places the Cretaceous Tropic Shale against the Jurassic Co-op Creek member of the Carmel Formation. The fault to the east (Fault L) accommodates a similar but lesser throw (~261 m; ~856 ft) (Figures 5 and 8). A third fault (Fault K) abuts faults A and L at a high angle, strikes ~N30°W, and dips ~75°NE (Figure 5). This fault places the Jurassic Crystal Creek Member of the Carmel Formation adjacent to the Jurassic Windsor Member with ~86 m (280 ft) throw. We propose that this fault intersects Fault L at a depth of 335 m (1100 ft) (cross-section N–N′; Figures 8 and 10) and likely aids in the transfer of strain between Faults A and L. At this latitude, the central Sevier fault zone accommodates a total of ~712 m (2340 ft.) throw, lower than estimates to the south.

The northernmost Central Domain displays three faults in map view and the northward projection of Fault A (Figure 5). The two easternmost, subparallel faults (Faults L and M) merge at a low angle in map view, forming a fault-bound slice or lens, and have attitudes of approximately N40°E, ~85°NW (Figure 5). Fault M juxtaposes Jurassic Navajo Sandstone and the Jurassic Co-op Creek Member of the Carmel Formation, while Fault L juxtaposes the Co-op Creek Member of the Carmel Formation and the Cretaceous Dakota Sandstone. Fault M may have once been the main strand of the fault, but local stress field changes or fault interactions at depth may have shifted slip accommodation to Fault L.

6.3. Northern Domain. The Northern Domain is located between the city of Glendale and the northern boundary of the mapped area (Figure 4). In contrast to the Southern and Central domains, the central Sevier fault is predominantly a single-strand fault (Fault O) throughout the Northern Domain (Figure 4). The main strand of the Sevier fault strikes ~N40°E and dips 76–81°W. The total throw across the Northern Domain of the Sevier fault zone decreases northward from ~525 m (1720 ft) at cross-section O–O′ and ~465 m (1530 ft) at cross-section P–P′ to ~396 m (1300 ft) at cross-section Q–Q′ and ~412 m (1350 ft) at cross-section R–R′ (Figures 4 and 11).

Eight faults, named Fault Group N, are exposed to the east-northeast of Glendale (Figure 4). Group N faults can be divided into NNW- and NNE-striking fault sets with one NE-striking cross-fault. Dips range from 58–81°W. The total throw across these faults is ~525 m (1720 ft) (cross-section O-O′; Figure 11). The western splay connects with the main strand of the Sevier fault (Fault L) at the surface (Figure 4). However, more importantly, the NE-striking, steeply northwest-dipping cross-fault is a splay of Fault L that abuts Fault O at its northwest termination (Figure 4). This fault links the main strands of the Sevier fault (Faults L and O) at an abrupt right step. This cross-fault juxtaposes the Jurassic Co-op Creek Member of the Carmel Formation against the Cretaceous Dakota Sandstone and is the main strand of the Sevier fault for its entire ~750 m (2460 ft) length.

Fault Group P lies just to the west of a bend in the main strand of the Sevier fault and comprises five hanging wall faults: three W-dipping, one E- to SE-dipping, and one non-planar fault with NW- and N-dipping sections (Figure 4 and section P–P′ in Figure 11). Group P faults offset units as young as the Cretaceous Kaiparowits/Wahweap Formations (Figure 3) at the surface. We determined the geometry of several of these faults, covered by Quaternary alluvium in Dry Wash Canyon and its tributaries (Figure 4), based on mapped outcrop relationships as well as requirements for cross-section restorations across this latitude of the Northern Domain. The W-dipping faults generally strike N25°E and dip 79°–85°W. The three western faults likely connect at depth and in map view appear to abut the E-striking fault in Dry Wash Canyon at the surface (Figure 4). Thus, we suggest that this east-striking fault may be a transfer fault.

Between the labels for Fault O in Figure 4, the map-view trace of the Sevier fault forms a large bend with strikes that vary, from south to north: N70°E, N20°E, and N5°E. The throw across this trace of the fault is ~318 m (~1040 ft) (section P–P′ in Figure 11). The main strand of the Sevier fault is interpreted to connect at depth with the two easternmost faults within Fault Group P (Figure 11). The total throw across Group P faults and the main fault strand is ~465 m (1530 ft). North of Fault Group P, the Sevier fault strikes ~N35°E and dips 76°W and displays a relatively constant orientation northward to the latitude of cross-section Q–Q′, where it accommodates ~396 m (1300 ft) throw (Figure 11).

Along the Sevier fault, pre-Claron Formation units have a general north-northwest dip (1°, 19°) except in fault blocks or close to faults. Cross-sections Q–Q′, and R–R′ (Figure 11) show an anticline in the hanging wall of the main strand of the Sevier fault. In addition to this anticline, several regional folds exist near the study area (Figure 1).

Four faults, here named Fault Set Q, cut a Quaternary basalt flow (Qb) near Black Mountain (Figures 4 and 11), the youngest offset unit in this study (see *Temporal constraints on fault displacement*). Three of these faults strike N44°E. One dips 82°SE and the other two dip ~80° NW, and together, these faults accommodate ~412 m (1350 ft) throw

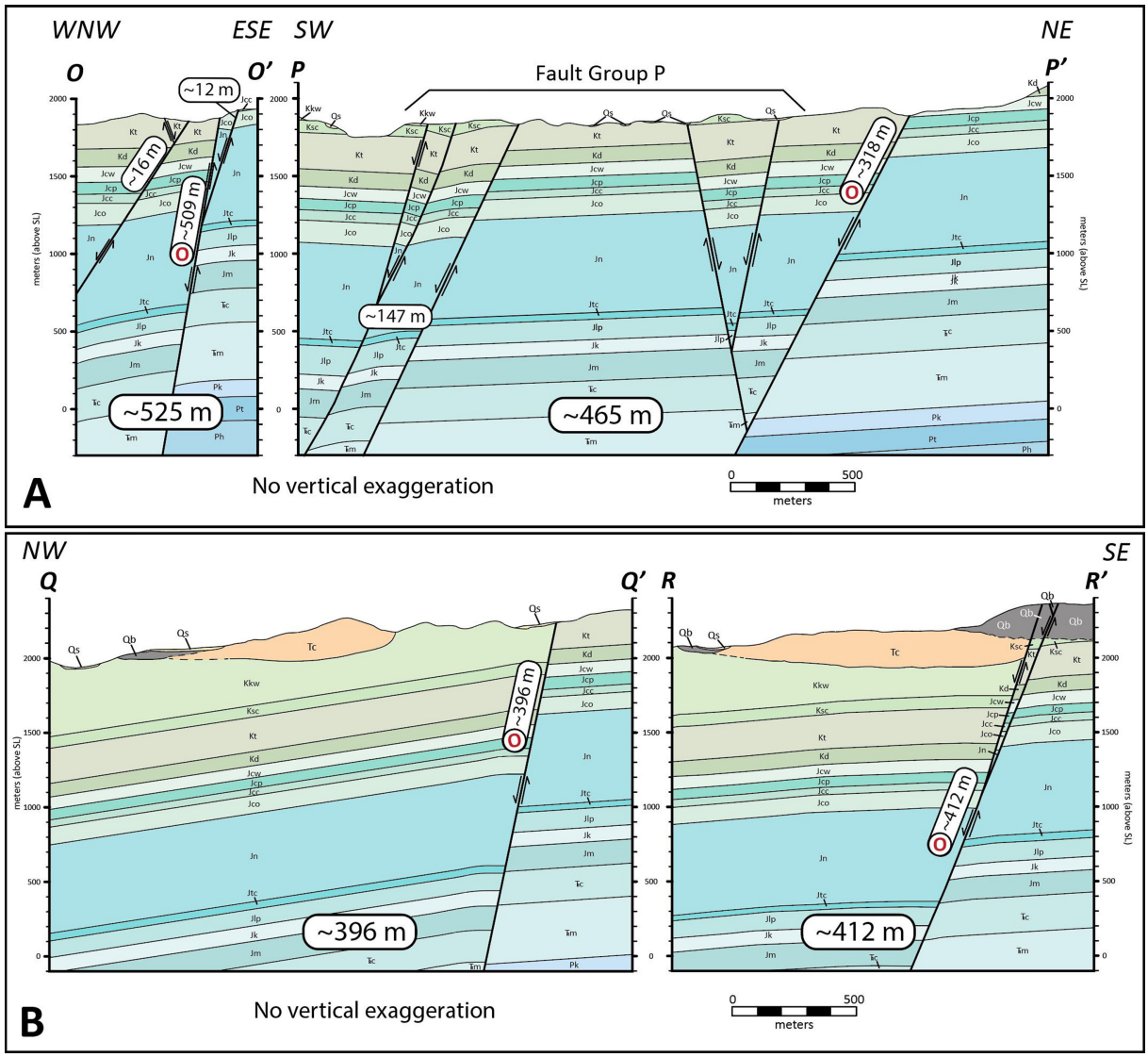

Figure 11: Cross-sections O-O′ through R-R′ from the Northern Domain of the Sevier fault zone study area. We display total fault stratigraphic throw values in white boxes on each section. (a) Cross-sections O-O′ and P-P′, constructed along WNW-ESE and SW-NE lines of section, respectively (Figure 4). (b) Cross-sections Q-Q′ and R-R′, constructed along NW-SE lines of section (Figure 4). See Figure 3 for the complete names of all stratigraphic unit abbreviations. All cross-sections constructed with no vertical exaggeration.

(section R–R′ in Figure 11). The fourth fault is a cross-fault with an attitude of N82°E, 80°N, and displays ~1 m (~3 feet) of throw. The total post-basalt flow emplacement throw accommodated by Set Q faults is ~3 m (~10 feet).

6.4. Temporal Constraints on Fault Displacement. We sampled and dated two basalt samples (BRC-1 and BRM-2) from the northern portion of the Northern Domain (Figure 4; online Supplementary Materials 1 and 2). One sample was collected from the Sevier fault hanging wall at Black Rock Canyon, and the other sample was collected from the footwall at Black Mountain. The sample from Black Rock Canyon yielded a $^{40}Ar/^{39}Ar$ isochron age of 564 ± 20 ka, and the sample from Black Mountain yielded an $^{40}Ar/^{39}Ar$ isochron age of 580 ± 50 ka (Figure 12) [48]. These dates were calculated prior to changes in the fluence age and decay constants. The isochron ages are 570 +/- 20 ka (BRC-1) and 586 +/- 50 ka (BRM-2) when recalculated assuming a fluence monitor age of 28.201 ka : 570 +/- 20 ka (BRC-1) and 586 +/- 50 ka (BRM-2) when recalculated assuming a fluence monitor age of 28.201 Ma [124]. These ages are similar to the 560 ka ± 70 ka K-Ar date determined by Best et al. [125] for volcanic rocks in Black Rock Canyon and place a maximum age of ~570 ka for the latest displacement along the central Sevier fault in the northernmost region within our study area.

If we use the ~3 m throw of the ~570 ka basalt flow, we constrain the post-570 ka slip rate to ~0.005 mm/y along the Sevier fault at the northernmost extent of our study area. This value is lower than Hecker's [81] estimate (0.360 mm/y) for the Spencer Bench segment of the Sevier fault at Red Canyon approximately 20 km north of the study area. However, it is possible that undocumented faults east or west of the main trace have accommodated some portion

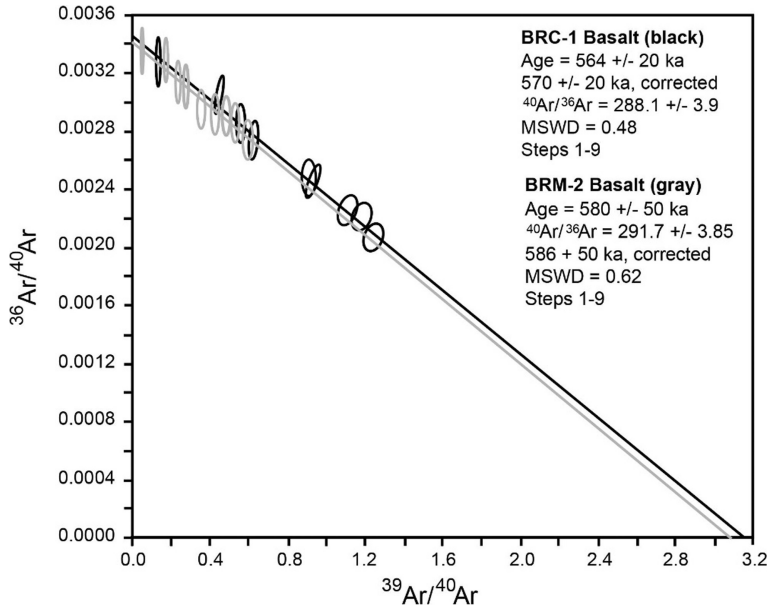

Figure 12: Isochron data from the Black Rock Canyon basalt and Black Mountain basalt (see Figure 4 for sample locations). Nine hour heating steps were used for each sample to determine the isochron age (ellipses indicate uncertainty). The Black Rock Canyon basalt (BRC-1) is shown in black and the Black Mountain basalt (BRM-2) is shown in gray. The original dates are from Schiefelbein [48].

of the total extension near Black Mountain or that the fault had more slip events to the north. In addition, we cannot constrain any changes in slip rate since 570 ka.

6.4.1. Faulting Within Quaternary Sedimentary Deposits. No Quaternary conglomerate units in the study area are cut by a fault at the surface. This suggests that either surface ruptures are older than the conglomerate units along those sections of the fault zone or these deposits are not located on faults. The latter scenario is more probable because none of the fault strands in the area of interest project under the conglomerate. However, several of the conglomerate outcrops are tilted, which may indicate nearby faulting.

7. Discussion

Although multipartite linkage zones have been mapped and described in the past [34, 39, 40, 126–130], we present the evolution of an unusually complex normal fault zone that displays a range of structures that help accommodate extension. Our data reveal that different types of segment linkage resulted in the fault network of the Southern and Central Domains. Within these linkage sites, relay ramps with classic ramp monoclines formed (Figures 2(e) and 5), but we also documented fault parallel folds within ramps. Together, these multiple linkage sites form a structural salient, here called the Orderville salient. Because of the excellent exposure along strike, our data permit us to deepen understanding of how fault segment linkage geometries evolve in extensional systems, which can be especially useful in unexposed or poorly exposed subsurface segmented fault networks.

7.1. Complex Fault Linkage Within the Central Sevier Fault Zone. We propose that originally isolated faults linked in the Southern and Central Domains to form the most complex portion of the central Sevier fault zone (Figures 4 and 5). The bordering fault segments along strike are the Mt. Carmel fault segment (Fault A) in the south and the Spencer Bench segment (Fault L/O) in the north. These west-dipping, synthetic normal faults are in a right-stepping, en echelon relationship. To evaluate how the accommodation of extension changes along strike, we constructed a total fault throw vs. distance diagram from south to north, measured parallel to fault strike (Figure 13). Our data suggest that total throw accommodated by the Mt. Carmel segment in the south is ~790–860 m, while the Spencer Bench segment has only accommodated ~400–525 m total throw.

A relatively steep displacement gradient (~60 m/km) occurs primarily in the Central Domain (Figure 13), where we suggest that slip and strain transfer between the primary faults resulted in the present-day fault network. In the Central and Southern Domains, we identified several different linkage styles, including soft linkage and a range in overlapping hard linkage styles (Figure 2(a)–2(d)). The resulting geometry of the Orderville salient is far more complex than when just two faults interact [51].

7.2. Fault Capture in the Southern Domain. Near Orderville, we suggest that segments of the central Sevier fault linked by fault capture with a breakthrough fault, a type of hard linkage, based on geometries that indicate a relay ramp, the map-view fault trace pattern, and the along-strike change of the largest amount of slip between Faults A and B using fault C. The total throw accommodated by faults A and B is

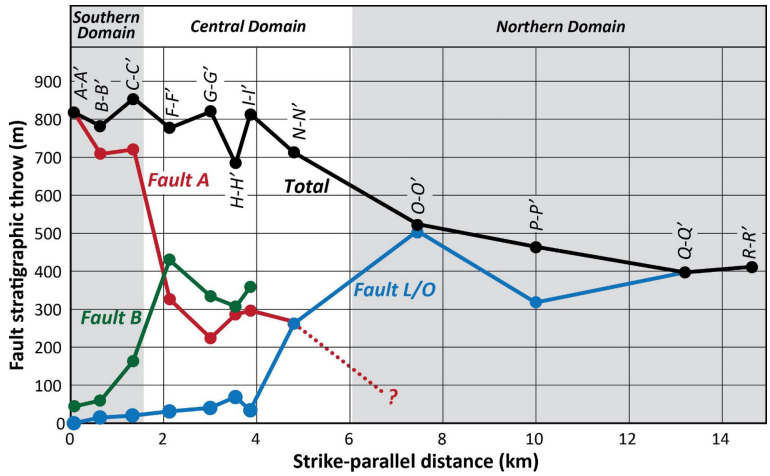

FIGURE 13: Fault stratigraphic throw vs. strike-parallel distance for the primary strands of the central Sevier fault zone. Lines of section used to constrain displayed values are in italics adjacent to the total stratigraphic throw line (in black).

higher in the south at ~785–856 m (sections A–A′, B–B′, and C–C′; Figure 6) and decreases to ~749 m at the termination of the relay ramp at section F–F′ (Figure 13).

We hypothesize that as Faults A and B accumulated displacement and propagated laterally, the Orderville relay ramp formed between the fault segments (Figures 2(e) and 5). The fault-parallel syncline formation is addressed below. The fault trace pattern of Faults A and B (Figure 6) closely resembles the most advanced stage in idealized models of fault capture (Figure 2(c)), where B terminates against A at the top of the ramp (Figure 5) and linkage by breakthrough faults (Figure 2(d)), where we suggest that unexposed Fault C broke through at the base of the ramp, hard linking Faults A and B (Figure 5).

7.3. Overlapping Fault Interactions in the Central Domain. We consider the Stewart Canyon overlap zone of the Central Domain to be a complex slip and strain transfer zone, with four major linked, overlapping faults (A, B, F, and L) and a more complicated geometry than the simpler fault capture linkage of the Southern Domain. This transfer zone involves at least twelve faults, four sites of linkage, and three relay ramps. We subdivide the Stewart Canyon overlap zone into the East, Central, and West overlap zones for ease of description.

7.3.1. East Stewart Canyon Overlap Zone. Based on displacement and map patterns, Fault L is the main fault in the eastern zone, especially near the northern extent of the Central Domain (Figures 5 and 13), and the East Stewart Canyon relay ramp formed between overlapping Faults L and *F* (Figure 5). Where Faults F and L are subparallel in strike and overlap at sections H–H′ and I–I′ (Figure 5), the total throw accommodated by both faults is ~86–95 m (Figure 8). To the north of the overlap zone, Fault L displays an increase in throw to over 260 m (section N–N′; Figure 8), while Fault F displays a northward change in strike from ~N40°E to ~N near the linkage site with Fault B (Figure 5). Both faults display a southward decrease in displacement within the overlap zone; Fault F displays a decrease from ~27 m throw (section I–I′; Figure 8) to zero at the mapped fault tip (Figure 6), and Fault L displays a decrease from ~43 m (section H–H′; Figure 8) to less than 30 m near the mapped tip of fault F (Figure 5). Although both faults display a decrease in displacement to the south in the region of overlap, we suggest that the greater displacement gradient accommodated by Fault L resulted in the north-dipping relay ramp between Faults L and F.

The map-view bounding fault geometries, the north-dipping relay ramp, and along-strike displacements indicate near-surface soft linkage of overlapping Faults L and F, similar to the idealized map-view diagram displayed in Stage 2 of Figure 2(c). With greater accumulated displacement, we suggest that these faults would display hard linkage at the surface; in fact, we posit that their relatively close spacing suggests they likely hard link at depth.

7.3.2. Central Stewart Canyon Overlap Zone. Based on displacement distribution and surface fault geometries, we interpret that Faults F and B likely formed the central Stewart Canyon relay ramp by a combination of atypical fault capture (Figure 2(c)) and breakthrough fault linkage (Figure 2(d)). Overlapping Faults F and B formed the central Stewart Canyon overlap zone via hard linkage accommodated by a combination of fault capture of Fault B by Fault F and a base breach of the relay ramp by cross-Fault D, which also Faults B and F (Figure 5). The attitudes of bedding within the ramp reveal a typical ramp monocline as well as a NE-plunging anticline, which we address below (Figure 5).

Within the Central Stewart Canyon relay ramp, Fault B, the main strand of the Sevier fault, accommodates a far greater throw than Fault F at every latitude (cross-sections G–G′, H–H′, and I–I′; Figures 5 and 8). Fault F displays a northward increase in throw from zero at its tip to ~27 m at section I–I′ (Figures 5 and 8), and Fault B displays a relatively constant throw from~333 m in the south (cross-section G–G′) to ~308 m at cross-section H–H′ to ~359 m at the latitude of line of section I–I′. At that latitude, the total throw across Faults B, D, and F is ~424 m.

We propose that the significant difference in total displacement between Faults B and F and the relative timing revealed by the abutment of Fault B into Fault F provide evidence that: (1) slip along Fault F south of the abutment intersection likely ceased or significantly decreased after the Fault B abutment into Fault F; alternatively, slip was transferred onto Fault F; and (2) the segment of Fault F north of that intersection became the main strand of the Sevier fault after that event.

The throw accommodated by or the geometry of Fault F must have been significant enough to provide a barrier to the propagation of the tip of Fault B. Because Fault F accommodates less than 100 m (328 ft) total throw at the F-B intersection today, the slip accommodated by Fault F at the time of abutment may have been similar to the present day. At the moment of abutment, by definition, the tip of Fault B would have displayed zero displacement [12], so the shallow north dip of the relay ramp between Faults F and B, in the hanging wall of Fault F, was likely already established, caused primarily by the displacement gradient along fault F (a scissor fault from its tip to the abutment intersection). However, it is possible that Fault F continued to accommodate minor slip after Fault B became the dominant bounding fault (Figure 6). Once Fault B abutted F, we propose that nearly all future strain was accommodated by Fault B and the north segment of fault F, resulting in the present-day difference in fault throw. After fault B became the dominant bounding fault, we suggest that Fault D formed, helping to accommodate the local stresses near the abutment intersection (Figure 5).

7.3.3. West Stewart Canyon Overlap Zone. We suggest that the West Stewart Canyon relay ramp formed as overlapping Faults A and F/B–C hard-linked at two sites, one to the north (Fault F) and one to the south (Fault B–C), with later cross-faults I and J that abut Faults A and B (Figure 5). Because these Faults (A and B) also interacted to the south, forming the Orderville relay ramp, cross-fault C likely had formed early in the history of the West Stewart Canyon overlap zone. The map pattern for the West Stewart Canyon overlap zone shows a lens shape, similar to the idealized hard linking of overlapping faults (Figure 2(b)). However, because these faults have accommodated most of the fault throw across the Sevier fault zone at this latitude after linking, any early displacement deficit at the time of linkage cannot be documented today. We propose that fault spacing was small enough to allow the two faults' stress fields to interact with each other, and because these faults have similar displacements (and likely northward lateral propagation direction and slip rates), the faults linked via overlapping linkage rather than fault capture.

7.4. Formation of Folds Within Relay Ramps. The Orderville relay ramp contains a fault-parallel syncline and the Central Stewart Canyon relay ramp contains a fault-parallel anticline (Figure 5). The stratigraphy outside of the relay ramps are generally flat lying or very gently west dipping. If these folds formed by normal or reverse drag along the bounding faults, the beds *proximal* to the fault would 'roll-over' and dip more steeply towards or away from the fault. Similarly, if the folds resulted from fault propagation [131, 132], the beds on both sides of the fault would be deformed. However, we observe none of these geometries proximal to these relay ramps.

If synthetic bounding faults merge at depth, there will be a downward decrease in distance between the bounding faults. When ramp-bounding faults originally linked, we suggest that rocks within the ramps likely exhibited the classic ramp monocline (Figure 2(e)), but we know of no syn-ramp-formation mechanism that would create a long, fault-parallel fold within a relay ramp that displays an axis parallel to the dip direction of the monocline. However, if either or both bounding faults slip after relay ramp formation, the rocks within the fault-bounded, wedge-shaped block may be deformed due to the interactions of the bounding faults at depth, with increasing fold tightness occurring with increasing accumulated displacement along the bounding faults and, possibly, with proximity to the fault intersection at depth.

Based on these observations, we suggest that the bounding faults of both the Orderville and Central Stewart Canyon relay ramps likely merge at depth and have accommodated significant post-linking displacement, resulting in these fault-parallel folds. Additionally, in the case of the plunging anticline within the central Stewart Canyon relay ramp, the axial trace of the fold changes trend to the northeast (Figure 5). This map-view observation supports our view that the ramp-bounding faults likely change strike and/or dip with depth, thus causing the bend in the axial trace of the anticline.

7.5. Evolution of the Orderville Salient Fault Complex. We use the new data and analyses presented here to posit the following evolution of fault propagation and linkage along the central Sevier fault zone (Figure 14). Although this reconstruction is non-unique, it provides a chronology of fault zone development that honors all fault trace geometric patterns, fault terminations, cross-cutting relations, relay ramp locations and geometries, and displacement-distance relations.

During Stage 1 (Figure 14(a)), the central Sevier fault initiated as six isolated faults, from south to north: the Mt. Carmel segment (Fault A), Fault B, Fault F, the Spencer Bench segment (Fault L); and two segments, Faults A′ and B′. To the north, the right-stepping, en echelon arrangement is consistent with stress interactions between the two main segments of the fault system (Faults A and L) interacting at depth, even if only by soft linkage. Additionally, the abrupt northward change in strike of fault A from ~N to NE, might indicate the influence of a pre-existing Laramide age [42, 79] structure on the propagation of fault segments or that Fault A is formed by a linkage of two differently striking sections.

During Stage 2 (Figure 14(b)), all faults continued to accumulate displacement and propagated along strike north and south. Faults A and A′ linked and Faults B and B′ linked to form Faults A and B, respectively, and overlapped and interacted by soft linkage, forming the north-dipping

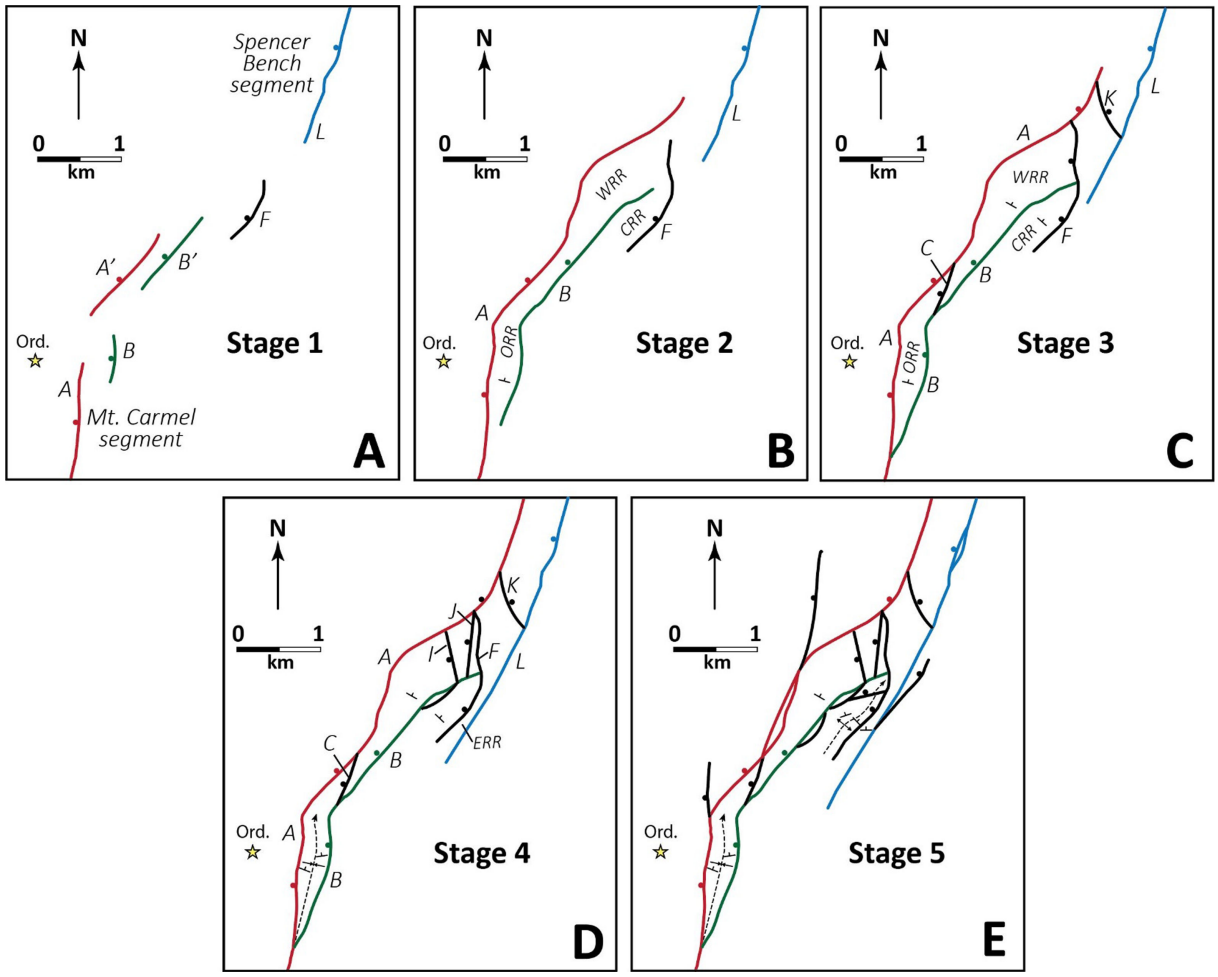

Figure 14: Simplified fault-trace diagrams displaying the hypothetical evolution of the central Sevier fault zone across the Southern and Central Domains. Use the fault map displayed in Figure 5 for reference. Fault colors match those in Figure 13. (a) Stage 1: two isolated, right-stepping, en echelon fault segments (Faults B and F) form between the Mt. Carmel (south) and the Spencer Bench (north) segments. (b) Stage 2: faults propagate laterally as displacement accumulates, forming the Orderville (ORR), West Stewart Canyon (WRR), and Central Stewart Canyon (CRR) relay ramps. (c) Stage 3: faults continue to accumulate displacement, propagate laterally, and begin linking. The ORR and WRR are breached at the base and top, and CRR bounding faults link at the base of the CRR. Fault K forms, hard linking the Mt. Carmel and Spencer Bench segments. (d) Stage 4: accumulated displacement along ORR bounding faults forms a N-plunging syncline subparallel to those faults, the East Stewart Canyon relay ramp (ERR) forms, and west-dipping cross-faults form near the base of the WRR. (e) Stage 5: splay faults form and propagate, the NE-plunging anticline in the CRR forms, and cross-fault D forms near the base of the CRR. In essence, this fault complex is a transfer zone between the primary fault segments, with all relay ramps displaying NNE dips, consistent with a ramp formed between two NE-striking, right-stepping, synthetic normal faults. Yellow star represents the city of Orderville (Ord.).

Orderville relay ramp monocline. To the north, Faults A, B, and F interacted and may have begun forming the West and Central Stewart Canyon relay ramps between them. In addition, Fault F propagated toward Fault A, and Fault B propagated toward Fault F (Figures 5 and 14(b)).

By Stage 3 (Figure 14(c)), as displacements along segments continued to accumulate, Fault A captured Fault B, and Fault C breached the base of the Orderville relay ramp. We suggest that the dip of the Orderville relay ramp continued to increase at least until the base and top breaches occurred (Figure 2(e)). Farther north, Fault F propagated and abutted Fault A, and Fault A continued to propagate northward and hard-linked with Fault L vis cross-fault K (Figures 5 and 14). As these displacements accumulated, the NNE dips of West and Central relay ramp monoclines increased. Based on cross-sectional data, once these abutments occurred, the segment of Fault F north of the Fault B abutment intersection became the dominant fault at that latitude, while Fault F south of that intersection accommodated minimal to no new displacement. This transfer of slip from an abutting fault onto an earlier fault is consistent with previous studies [38, 133, 134].

We suggest that the hard linkages that occurred during Stage 3 effectively linked all major segments across the Central Central Domain, thus permitting a more efficient accommodation of slip than prior to those linkages. In other words, more energy is required for the propagation of fault planes through intact rock relative to the energy

required to accommodate slip along existing faults [135–137]. We also posit that after this stage of hard linkage across most of the transfer zone between the primary segments (Mt. Carmel and Spencer Bench segments), it is likely that progressive strain localization has occurred, with the linkage zone evolving from one with more distributed deformation across a broad fault network between the main segments to a system of faults where the most active slip is accommodated by a connected series of faults [38] represented by the "main fault trace" indicated in Figure 5.

By Stage 4 (Figure 14(d)), Faults A and L continued to propagate laterally as displacements accumulated, and the East Stewart Canyon relay ramp formed between Faults L and F. Cross-faults I and J formed at the base of the West Stewart Canyon relay ramp in response to the significant stresses and resulting strain associated with the focus of new displacement along nearby Faults B, F, and A (see main fault trace in red on Figure 5). Finally, as displacements accumulated along bounding Faults A, B, and C, a bounding-fault-parallel N-plunging syncline formed in the Orderville relay ramp (Figure 14(d)).

During the final stage (Stage 5, the modern fault-trace map), displacement continued to accumulate, resulting in the formation and propagation of splay faults from Faults A and L, and cross-fault D deformed the base of the Central Stewart Canyon relay ramp (Figure 14(e)). In addition, a NE-plunging anticline formed between the bounding faults of the Central Stewart Canyon relay ramp. By this stage, in the present day, we suggest that any displacement deficits that existed soon after fault linkages across the overlap zone [35, 36] are no longer obvious in our cross-section constructions. As hard-linked faults accumulate displacement after linkage, relative displacement minima associated with the linkage type become difficult or even impossible to discern [10, 53, 138, 139].

7.5.1 Implications for Segmented Fault Growth, Seismic Hazards, and Geothermal Energy Potential. The en echelon arrangement of the Mt. Carmel and Spencer Bench segments is typical of normal fault segments in fault zones that have experienced one phase of extension [40, 61, 140]. In fact, most major normal faults worldwide have evolved from early initiation of segments that kinematically interact with one another forming complex zones of linkage that accommodate displacement, as opposed to unsegmented planar faults [37, 39, 41, 61, 62]. Although we cannot determine whether these two segments of the Sevier fault zone initially formed and propagated laterally as isolated, semi-elliptical faults (Figure 2(e)) [12] or as splays from a deeper fault [41, 61], the complex faulting of the Orderville salient displays a range of features consistent with the accommodation of strain in transfer zones between major en echelon normal fault segments [37, 39, 41, 61, 62].

The Central Domain contains (1) dominant NNE-striking relatively long faults and (2) many shorter, obliquely striking fault segments (Figure 5). These shorter faults predominantly breach relay zones between NNE-striking faults, consistent with previous studies of major normal fault systems [40, 136]. All four relay ramps dip ~NNE and formed between synthetic, WNW-dipping normal faults (Figure 5), consistent with the ramp dip direction expected between right-stepping, en echelon normal fault segments. However, the displacements of bounding faults for these ramps vary significantly, resulting in an unbreached relay ramp (East Stewart Canyon, with low bounding fault displacements), a base-breached relay ramp (Central Stewart Canyon, with moderate bounding fault displacements), and two base- and top-breached relay ramps, both associated with the western-most faults in the transfer zone, which display the greatest bounding-fault displacements.

Based on the relatively smooth transition of accumulated displacements from the higher values of the Southern Domain to the lower values of the Northern Domain (Figures 13 and 14), we suggest that these segments have now effectively hard-linked through the Orderville salient fault network, exhibiting no displacement deficits that might suggest an immature linkage zone [30, 31]. Interestingly, the zone of highest displacements projects along strike of the Mt. Carmel segment, on the western margin of the salient, with the step in high displacement values only taking place near the northern limit of the Central Domain.

Fault system discontinuities like that documented here may localize strain, act as barriers to fault rupture propagation, and may impact the location of earthquake foci and rupture propagation [10, 46, 48, 71, 137]. Our analysis indicates that early in the evolution of the salient, the Mt. Carmel and Spencer Bench segments were likely connected by soft linkage. During that period, we posit that the salient behaved as a significant barrier to the propagation of slip during earthquake events, with much of the energy associated with slip propagation absorbed at the boundary due to initiation and propagation of small fault segments and associated fractures between the primary segment [47, 57, 138]. Prior to hard linkage, the significant difference in displacements between the segments (Figure 14) was likely well-established, with a displacement deficit at the latitude of the linkage zone.

As displacement accrued and the complex fault segments accommodated strain and slip between those segments, the segments hard-linked, so that the fault system could now behave as a more continuous system, consistent with studies at other localities [49, 51, 134, 141]. However, any earthquake slip propagation from north or south would still be accommodated by multiple non-planar faults that exhibit a significant right step (near Fault K; Figure 5), suggesting that the northern margin of the Stewart Canyon overlap zone likely remains a structural and geometric barrier to fault-rupture propagation.

The northward decrease in total slip along the Sevier fault, both regionally [37, 38, 40] and locally (this study), would support a model where seismic hazard also decreases northward in concert with the decrease in displacement. Although fault-rupture propagation associated with a major earthquake near the Orderville salient would likely propagate through the barrier due to the hard linkage between segments [51, 139], it is likely that smaller magnitude earthquakes or slip from more distant

earthquakes on the Sevier fault system might be significantly impeded or even arrested [69, 70] by the fault complex documented here.

As faults evolve from individual faults/segments into a linked fault the scaling relationship of displacement (e.g., stratigraphic throw) to length changes dramatically at the time of linkage. Relatively high ratios of displacement to distance drop to lower values at that time. Thus, with time, the fault would fall into different positions on graphs of displacement:length for populations of faults [e.g., 26, 29, 59, 60]. The Sevier fault segments discussed here display ~400–850 m displacement and are 10's of km in length, but when linked are ~100 km in length. These displacement values fall within the range suggested for populations of medium- to large-length faults [cf., 26], both linked and unlinked. This relation suggests that the well-exposed, complex linkage zone described here may be more typical of major normal fault systems than generally documented.

Productive geothermal systems are strongly reliant on fracture permeability caused by magmatic and tectonic processes [140, 142]. As fluids circulate through geothermal systems, fault-related fracturing provides the best migration pathways both vertically and horizontally [22, 143, 144]. In a system like that documented in this study, with segments that have propagated, linked, and accommodated displacement [22, 145, 146], we would predict a broad zone of enhanced permeability that extends for several kilometers both parallel to and perpendicular to the fault trace. We suggest that the complexly linked fault zone geometries and evolution described here provide researchers with an example that might elucidate possible fault geometries in blind geothermal systems associated with major normal fault systems worldwide.

8. Conclusions

We have provided a model for the detailed evolution of a multipartite linkage zone between synthetic, en echelon segments of the central Sevier normal fault, which helps accommodate extension across the Basin and Range–Colorado Plateau transition. Our results yield the following conclusions.

(1) Multiple relay ramps of varying finite maturity helped accommodate strain and slip between two primary segments with different accumulated displacements. Although the relay-ramps bounding faults are subparallel to the primary segments, cross-faults that breached those relay ramps are commonly at a high angle to those earlier-formed faults.

(2) The NNE dip of all relay ramps in the study area is consistent with the dip expected between faults in a right-stepping en echelon geometry despite the complexity of the system.

(3) This linkage zone began as a soft-linked, en echelon system with a significant displacement deficit (relative to the primary faults to the north and south) and would have been a barrier to the propagation of slip across a range of earthquake magnitudes.

(4) As displacement along the linking fault system increased, a complex fault network eventually hard-linked the two primary faults, and the Orderville salient no longer exhibited a displacement deficit but instead displayed a transition in displacements from the higher displacement Mt. Carmel segment to the lower displacement Spencer Bench segment.

(5) Although it likely remains a structural and geometric barrier to fault rupture propagation in small (or distant) earthquakes, the Orderville salient would be unlikely to impede propagation associated with a nearby, major (>5.0 magnitude) earthquake.

(6) We think that the model of complex fault network evolution documented in this study can be used by researchers evaluating the potential of blind geothermal systems in structurally similar scenarios.

This well-exposed, complex fault linkage zone provides important spatial information about normal fault transfer zones that can be used to assess similar subsurface structures, especially for those investigating geothermal energy potential, groundwater flow, natural gas and oil reservoirs, mineral deposit formation, or seismic hazards.

Data Availability

All data are saved on computers (with cloud back-up) with the authors. New map data were compiled in a GIS database, and all stereographic projections and analyses were performed using the computer software GEOrient. Data associated with this manuscript are also included in the 2002 University of Nevada Las Vegas MS thesis by I. Schiefelbein [48] (now I. Schiefelbein Kerscher) and in the Supplemental Material.

Conflict of Interest Disclosure

The authors have no conflicts of interest to declare.

Acknowledgments

Thanks to Demi Durham of Trinity University, who performed 3D computer modeling to test the integrity of our cross-section constructions. Thanks also goes to Gene Smith, Terry Spell, and Barbara Luke for their helpful reviews of early drafts of this work and to Treasure Bailey for her assistance with field data collection. We thank Kathy Zanetti and Terry Spell of the Nevada Isotope Geochronology Laboratory for their assistance in obtaining age determinations. Finally, special thanks to Petroleum Experts, who generously donated use of the Move2022 software suite to Surpless and Trinity University.

Funding Statement

Funding was provided by the National Science Foundation [grant number 2042114] and two Keck Geology Consortium Advanced Research Project Grants which were part of an NSF-REU Award to the Keck Geology Consortium [grant number 1659322]. This work was also supported by funds from the Arizona/Nevada Academy of Science research grant, an American Association of Petroleum Geologists Grants-in-Aid, a Geological Society of America Research Grant, and a Sigma Xi Grant-in-Aid of research to Schiefelbein. To aid in cross-section analysis, Petroleum Experts generously donated the MOVE 2022 computer modeling suite to Trinity University for use by Durham, Surpless, and his research students.

Supplementary Materials

We include a text description of $^{40}Ar/^{39}Ar$ Methods for dating the two basalt samples discussed in the text. We also include the $^{40}Ar/^{39}Ar$ step-heating data in Supplementary Material 2, Table A. We also include a link to detailed geologic and structural data that the authors used to help interpret evolution of the Sevier fault network (see METHODS).

REFERENCES

[1] J. S. Tchalenko, "Similarities between shear zones of different magnitudes," *Geological Society of America Bulletin*, vol. 81, no. 6, 1970.

[2] R. E. Wallace, "Fault scarps formed during the earthquakes of October 2, 1915, in Pleasant Valley, Nevada and some tectonic implications," *U.S. Geological Survey Professional Paper*, 1984.

[3] D. P. Schwartz and K. J. Coppersmith, "Fault behavior and characteristic earthquakes: Examples from the Wasatch and San Andreas fault zones," *Journal of Geophysical Research*, vol. 89, no. B7, pp. 5681–5698, 1984.

[4] A. J. Crone and K. M. Haller, "Segmentation and the coseismic behavior of Basin and Range normal faults: Examples from east-central Idaho and southwestern Montana, USA," *Journal of Structural Geology*, vol. 13, no. 2, pp. 151–164, 1991.

[5] J. A. Cartwright, B. D. Trudgill, and C. S. Mansfield, "Fault growth by segment linkage: An example for scatter in maximum displacement and trace length data from the Canyonlands Grabens of SE Utah," *Journal of Structural Geology*, vol. 17, no. 9, pp. 1319–1326, 1995.

[6] D. C. P. Peacock, "Propagation, interaction and linkage in normal fault systems," *Earth-Science Reviews*, vol. 58, nos. 1–2, pp. 121–142, 2002.

[7] A. B. M. Tvedt, A. Rotevatn, C.-A.-L. Jackson, H. Fossen, and R. L. Gawthorpe, "Growth of normal faults in multilayer sequences: A 3D seismic case study from the Egersund Basin, Norwegian North sea," *Journal of Structural Geology*, vol. 55, pp. 1–20, 2013.

[8] C. A. L. Jackson, R. E. Bell, A. Rotevatn, and A. B. M. Tvedt, "Techniques to determine the kinematics of synsedimentary normal faults and implications for fault growth models," *Geological Society, London, Special Publications*, vol. 439, no. 1, pp. 187–217, 2017.

[9] K. Huang, G. Zhong, M. He, L. Liu, Z. Wu, and X. Liu, "Growth and linkage of a complex oblique-slip fault zone in the Pearl River mouth Basin, northern South China sea," *Journal of Structural Geology*, vol. 117, pp. 27–43, 2018.

[10] B. Surpless and S. Thorne, "Segmentation of the Wassuk Range normal fault system, Nevada (USA): Implications for earthquake rupture and Walker Lane dynamics," *GSA Bulletin*, vol. 134, nos. 1–2, pp. 39–59, 2022.

[11] D. C. P. Peacock and D. J. Sanders, "Geometry and development of relay ramps in normal fault systems," American Association of Petroleum Geologists Bulletin, vol. 78, pp. 147–165, 1994.

[12] J. G. Crider and D. D. Pollard, "Fault linkage: Three-dimensional mechanical interaction between echelon normal faults," *Journal of Geophysical Research*, vol. 103, no. B10, pp. 24373–24391, 1998.

[13] J. E. Faulds and R. J. Varga, "The role of accommodation zones and transfer zones in the regional segmentation of extended terranes," in *Accommodation zones and transfer zones; The regional segmentation of the Basin and Range Province: Geological Society of America Special Paper 323*, J.E. Faulds, and J.H. Stewart, Eds., 1998.

[14] P. Rowley, "Cenozoic transverse zones and igneous belts in the Great Basin, Western United States: Their tectonic and economic implications," in *Accommodation Zones and Transfer Zones: The Regional Segmentation of the Basin and Range Province: Geological Society of America Special Paper 323*, J.E. Faulds, and J.H. Stewart, Eds., pp. 195–228, 1998.

[15] A. Aydin, "Fractures, faults, and hydrocarbon entrapment, migration, and flow," *Marine and Petroleum Geology*, vol. 17, no. 7, pp. 797–814, 2000.

[16] W. Narr, D. S. Schechter, and L. B. Thompson, "Naturally fractured reservoir characterization," Society of Petroleum Engineers, Richardson, Texas, 2006.

[17] A. Brogi, M. C. Alçiçek, D. Liotta, E. Capezzuoli, M. Zucchi, and P. Matera, "Step-over fault zones controlling geothermal fluid-flow and Travertine formation (Denizli Basin, Turkey)," V. 89 *Geothermics*, vol. 89, p. 101941, 2021.

[18] K.-S. Kim, D. Peacock, and D. Sanderson, "Fault damage zones," *Journal of Structural Geology*, vol. 26, no. 3, pp. 503–517, 2004.

[19] J. E. Faulds, N. H. Hinz, G. M. Dering, and D. L. Siler, "The hybrid model-the most accommodating structural setting for geothermal power generation in the Great Basin, Western USA," *Geotherm. Resources. Council. Transactions*, vol. 27, pp. 3–10, 2013.

[20] N. H. Faulds and N. H. Hinz, "Favorable tectonic and structural settings of geothermal settings in the great Basin region, Western USA: proxies for discovering blind geothermal systems:," in *Proceedings, World Geothermal Congress 2015*, Melbourne, Australia, 2015.

[21] T. Sharmin, N. Khan, M. Akram, and M. Ehsan, "A state-of-the-art review on geothermal energy extraction, utilization, and improvement strategies: conventional, hybridized, and enhanced geothermal systems," *International Journal of Thermofluids*, vol. 18, p. 100323, 2023.

[22] J. Shervais, J. DeAngelo, J. Glen, et al, "Geothermal play fairway analysis, part 1: Example from the Snake River Plain, Idaho," *Geothermics*, vol. 117, p. 102865, 2024.

[23] D. Wells and K. J. Coppersmith, "New empirical relationships among magnitude, rupture length, rupture width, rupture area, and surface displacement," *Bulletin of the Seismological Society of America*, vol. 84, no. 4, pp. 974–1002, 1994.

[24] S. G. Wesnousky, "Displacement and geometrical characteristics of earthquake surface ruptures: Issues and implications for seismic-hazard analysis and the process of earthquake rupture," *Bulletin of the Seismological Society of America*, vol. 98, no. 4, pp. 1609–1632, 2008.

[25] S. Bennett, C. DuRoss, R. Gold, et al, "Paleoseismic results from the Alpine site, Wasatch fault zone: Timing and displacement data for six Holocene earthquakes at the Salt Lake City–Provo segment boundary," *Bulletin of the Seismological Society of America*, vol. 108, no. 6, pp. 3202–3224, 2018.

[26] A. Torabi and S. S. Berg, "Scaling of fault attributes: A review," *Marine and Petroleum Geology*, vol. 28, no. 8, pp. 1444–1460, 2011.

[27] R. K. Mark and M. G. Bonilla, "Regression analysis of earthquake magnitude and surface fault length using the 1970 data of Bonilla and Buchanan; Menlo Park, California: Department of the Interior Geological Survey," *Open File Report*, vol. 77–614, p. 9 , 1977.

[28] M. D. Zoback and S. M. Gorelick, "Earthquake triggering and large-scale geologic storage of carbon dioxide," *Proceedings of the National Academy of Sciences of the United States of America*, vol. 109, no. 26, pp. 10164–10168, 2012.10.1073/pnas.1202473109

[29] D. C. P. Peacock and D. J. Sanderson, "Displacements, segment linkage and relay ramps in normal fault zones," *Journal of Structural Geology*, vol. 13, no. 6, pp. 721–733, 1991.

[30] I. K. Koukouvelas and T. T. Doutsos, "Implications of structural segmentation during earthquakes: The 1995 Egion earthquake Gulf of Corinth," *Journal of Structural Geology*, vol. 18, no. 12, pp. 1381–1388, 1996.

[31] S. B. Pavlides, N. C. Zouros, F. Zhongjing, C. Shaoping, M. D. Tranos, and A. A. Chatzipetros, "Geometry, kinematics and morphotectonics of the Yanqing–Huailai active faults (northern China)," *Tectonophysics*, vol. 308, nos. 1–2, pp. 99–118, 1999.

[32] A. Gupta and C. H. Scholz, "A model of normal fault interaction based on observations and theory," *Journal of Structural Geology*, vol. 22, no. 7, pp. 865–879, 2000.

[33] J. G. Crider, "Oblique slip and the geometry of normal-fault linkage: mechanics and a case study from the Basin and Range in Oregon," *Journal of Structural Geology*, vol. 23, no. 12, pp. 1997–2009, 2001.

[34] D. A. Ferrill and A. P. Morris, "Displacement gradient and deformation in normal fault systems," *Journal of Structural Geology*, vol. 23, no. 4, pp. 619–638, 2001.

[35] S. Reber, W. J. Taylor, M. Stewart, and I. M. Schiefelbein, "The geologic transition, high plateaus to Great Basin - a symposium and field guide: Utah Geological Association Publication 30 and Pacific Section American Association of Petroleum Geologists guidebook," in *Linkage and reactivation along the northern Hurricane and Sevier faults, southwestern Utah, in Erskine*, M.C. Erskine, J.E. Faulds, J.M. Bartley, and P.M. Rowley, Eds., pp. 379–400, 2001.

[36] W. J. Taylor, M. E. Stewartward, R. L. Orndorff, et al, "The Geologic transition, high plateaus to Great Basin - a Symposium and field guide: Utah Geological Association Publication 30 and Pacific section American Association of Petroleum Geologists guidebook," in *Fault segmentation and linkage: examples from the Hurricane fault, southwestern U.S.A., in Erskine*, M.E. Erskine, J.E. Faulds, J.M. Bartley, and P.D. Rowley, Eds., 78th ed., 2001.

[37] G. Camanni, V. Roche, C. Childs, et al., "The three-dimensional geometry of relay zones within segmented normal faults," *Journal of Structural Geology*, vol. 129, p. 103895, 2019.

[38] C. Nixon, D. Sanderson, S. Dee, J. Bull, R. Humphreys, and M. Swanson, "Fault interactions and reactivation within a normal-fault network at Milne point, Alaska," *AAPG Bulletin*, vol. 98, no. 10, pp. 2081–2107, 2014.

[39] C. Nixon, J. Bull, and D. Sanderson, "Localized vs distributed deformation associated with the linkage history of an active normal fault, Whakatane Graben, New Zealand," *Journal of Structural Geology*, vol. 69, pp. 266–280, 2014.

[40] O. Duffy, R. Bell, C. Jackson, and R. Gawthorpe, "Fault growth and interactions in a multiphase rift fault network," *Journal of Structural Geology*, vol. 80, pp. 99–119, 2015.

[41] V. Roche, G. Camanni, C. Childs, et al, "Variability in the three-dimensional geometry of segmented normal fault surfaces," *Earth-Science Reviews*, vol. 216, p. 103523, 2021.

[42] G. H. Davis, "Structural geology of the Colorado Plateau region of Southern Utah," *Geological Society of America Special Paper*, vol. 342, p. 127, 1999.

[43] W. R. Lund, T. R. Knudsen, and G. S. Vice, "Paleoseismic reconnaissance of the Sevier fault, Kane and Garfield counties, Utah: Utah Geologic Survey Special Study 122," *Paleoseismology of Utah*, 31 , 2008.

[44] J. J. Anderson and P. D. Rowley, "Geologic map of the Panguitch NW Quadrangle, iron and Garfield counties,Utah" *Utah Geological and Mineral Survey Map*, vol. 103, p. 8 , 1987.

[45] H. H. Doelling, F. D. Davis, and C. J. Brandt, "The geology of Kane County, Utah," *Geology, Mineral Resources, Geologic Hazards: Utah Geological and Mineral Survey Bulletin*, vol. 124, p. 192 , 1989.

[46] R. E. Anderson and G. E. Christenson, "Quaternary faults, folds, and selected volcanic features in the cedar city 1°X2° Quadrangle," *Utah: Utah Geological and Mineral Survey Miscellaneous Publication*, vols. 89–6, p. 29 , 1989.

[47] R. B. Smith and W. J. Arabasz, "Seismicity of the Intermountain seismic belt," in *Neotectonics of North America: Geological Society of America*, D.B. Slemmons, E.R. Engdahl, M.D. Zoback, and D.D. Blackwell, Eds., pp. 185–228, 1991.

[48] I. M. Schiefelbein, "Fault segmentation, fault linkage, and hazards along the Sevier fault, Southwestern Utah," M.S. thesis, University of Nevada Las Vegas, 2002.

[49] S. A. Kattenhorn, A. Aydin, and D. D. Pollard, "Joints at high angles to normal fault strike: an explanation using 3-D numerical models of fault-perturbed stress fields," *Journal of Structural Geology*, vol. 22, no. 1, pp. 1–23, 2000.

[50] R. H. Sibson, "Earthquakes and rock deformation in crustal fault zones," *Annual Review of Earth and Planetary Sciences*, vol. 14, no. 1, pp. 149–175, 1986.

[51] D. A. Ferrill, J. A. Stamatakos, and D. Sims, "Normal fault corrugation: Implications for growth and seismicity of active normal faults," *Journal of Structural Geology*, vol. 21, nos. 8–9, pp. 1027–1038, 1999.

[52] P. Zhang, F. Mao, and D. B. Slemmons, "Rupture terminations and size of segment boundaries from historical earthquake ruptures in the Basin and Range province," *Tectonophysics*, vol. 308, nos. 1–2, pp. 37–52, 1999.

[53] I. Manighetti, C. Caulet, L. De Barros, C. Perrin, F. Cappa, and Y. Gaudemer, "Generic along-strike segmentation of Afar normal faults, East Africa: Implications on fault growth and stress heterogeneity on seismogenic fault planes," *Geochemistry, Geophysics, Geosystems*, vol. 16, no. 2, pp. 443–467, 2015.

[54] P. H. Larsen, "Relay structures in a lower Permian basement-involved extensional system, East Greenland," *Journal of Structural Geology*, vol. 10, no. 1, pp. 3–8, 1988.

[55] C. K. Morley, R. A. Nelson, T. L. Patton, and S. G. Munn, "Transfer zones in the East Africa rift system and their relevance to hydrocarbon exploration in rifts," *American Association of Petroleum Geologists Bulletin*, vol. 106, pp. 1143–1157, 1990.

[56] B. Trudgill and J. Cartwright, "Relay-ramp forms in normal-fault linkages, Canyonlands National Park, Utah," *Geological Society of America Bulletin*, vol. 106, no. 9, pp. 1143–1157, 1994.

[57] J. J. Walsh, J. Watterson, W. R. Bailey, and C. Childs, "Fault relays, bends and branch-lines," *Journal of Structural Geology*, vol. 21, nos. 8–9, pp. 1019–1026, 1999.

[58] D. C. P. Peacock, S. P. Price, A. G. Whitham, and C. S. Pickles, "The world's biggest relay ramp:Hold with Hope, NE Greenland," *Journal of Structural Geology*, vol. 22, no. 7, pp. 843–850, 2000.

[59] L. Maerten, E. J. M. Willemse, D. D. Pollard, et al., "Slip distributions on intersecting normal faults," *Journal of Structural Geology*, vol. 21, no. 3, pp. 259–272, 1999.

[60] A. Nicol, J. Watterson, J. J. Walsh, and P. A. Gillespie, "The shapes, major axis orientations and displacement patterns of fault surfaces," *Journal of Structural Geology*, vol. 18, nos. 2–3, pp. 235–248, 1996.

[61] H. Fossen and A. Rotevatn, "Fault linkage and relay structures in extensional settings—A review," *Earth-Science Reviews*, vol. 154, pp. 14–28, 2016.

[62] J. J. Walsh and J. Watterson, "Geometric and kinematic coherence and scale effects in normal fault systems.," Edited by A. M. Roberts, G. Yielding, and B. Freeman *Geological Society, London, Special Publications*, vol. 56, no. 1, pp. 193–203, 1991.

[63] R. L. Wheeler, "Persistent segment boundaries on Basin-Range normal faults: U.S," in *Geological Survey Open File Report OF 89-0315*, pp. 423–444, 1989.

[64] J. McCalpin, *Paleoseismology*, Academic Press, New York, 1996.

[65] M. E. Stewart and W. J. Taylor, "Structural analysis and fault segment boundary identification along the Hurricane fault in southwestern Utah," *Journal of Structural Geology*, vol. 18, no. 8, pp. 1017–1029, 1996.

[66] M. J. Young, R. L. Gawthorpe, and S. Hardy, "Growth and linkage of a segmented normal fault zone; the late Jurassic Murchison - Statfjord North fault, northern North Sea," *Journal of Structural Geology*, vol. 23, no. 12, pp. 1933–1952, 2001.

[67] S. U. Janecke, "Structures in segment boundary zones of the Lost River and Lemhi faults, east central Idaho," *Journal of Geophysical Research*, vol. 98, no. B9, pp. 16223–16238, 1993.

[68] C. M. dePolo and D. B. Slemmons, "Estimation of earthquake size for seismic hazards," Edited by E. L. Krinitzsky and D. B. Slemmons *Neotectonics in Earthquake Evaluation: Geological Society of America Reviews in Engineering Geology*, 1–28, 1990.

[69] I. Wong, W. Lund, C. DuRoss, et al., *Earthquake Probabilities for the Wasatch Front Region in Utah*, Utah Geological Survey Miscellaneous Publication, Idaho, and Wyoming, 2016.

[70] C. M. DePolo, D. G. Clark, D. B. Slemmons, and A. R. Ramelli, "Historical surface faulting in the Basin and Range province, Western North America: Implications for fault segmentation," *Journal of Structural Geology*, vol. 13, no. 2, pp. 123–136, 1991.

[71] E. A. Keller and N. Pinter, *Active Tectonics Earthquakes, Uplift, and Landscape*, Prentice Hall, Upper Saddle River, New Jersey, 1996.

[72] R. L. Bruhn, P. R. Gibler, and W. T. Parry, "Rupture characteristics of normal faults: An example from the Wasatch fault zone, Utah.," Edited by M. P. Coward, J. F. Dewey, and P. L. Hancock *Geological Society, London, Special Publications*, vol. 28, no. 1, pp. 337–353, 1987.

[73] C. M. Menges, "Late Quaternary faults scarps, mountain-front Landforms, and Pliocene-Quaternary segmentation on the range-bounding fault zone, Sangre de Cristo Mountains, New Mexico," Edited by E. L. Krinitzsky and D. B. Slemmons *Neotectonics in Earthquake Evaluation: Geological Society of America Reviews in Engineering Geology*, 131–156, 1990.

[74] H. D. Stenner, W. R. Lund, P. A. Pearthree, and B. L. Everitt, "Paleoseismologic investigations of the Hurricane fault in northwestern Arizona and Southwestern Utah," 99–8, *Arizona Geological Survey Open-File Report*, 1999.

[75] D. C. P. Peacock, "Displacements and segment linkage in strike-slip fault zones," *Journal of Structural Geology*, vol. 13, no. 9, pp. 1025–1035, 1991.

[76] R. Soliva and A. Benedicto, "A linkage criterion for segmented normal faults," *Journal of Structural Geology*, vol. 26, no. 12, pp. 2251–2267, 2004.

[77] A. J. Elliott, M. E. Oskin, J. Liu-Zeng, and Y. Shao, "Rupture termination at restraining bends—the last great earthquake on the Altyn Tagh fault," *Geophysical Research Letters*, vol. 42, no. 7, pp. 2164–2170, 2015.

[78] C. B. DuRoss, S. F. Personius, A. J. Crone, et al, "Fault segmentation: New concepts from the Wasatch fault zone," *Journal of Geophysical Research*, vol. 121, no. 2, pp. 1131–1157, 2016.

[79] P. E. Wannamaker, J. M. Bartley, A. F. Sheehan, et al, "The geologic transition, high plateaus to Great Basin - a symposium and field guide: Utah Geological Association Publication 30 and Pacific Section American Association of Petroleum Geologists guidebook," in *"Great Basin-Colorado*

Plateau transition in central Utah: an interface between active extension and stable interior," M.E. Erskine, J.E. Faulds, J.M. Bartley, and P.D. Rowley, Eds., 78th ed., pp. 1–38, 2001.

[80] B. C. Burchfiel and C. W. Hickcox, "Structural development of central Utah," in *Plateau - Basin and Range Transition Zone, 1972: Utah Geological Association*, J.L. Baer, and E. Callaghan, Eds., Central Utah, 1972.

[81] S. Hecker, "Quaternary tectonics of Utah with emphasis on earthquake-hazard characterization," *Utah Geological Survey Bulletin*, vol. 127, pp. 1–31, 1993.

[82] R. L. Armstrong, "Sevier orogenic belt in Nevada and Utah," *Geological Society of America Bulletin*, vol. 79, no. 4, 1968.

[83] W. R. Dickinson, M. A. Klute, M. J. Hayes, et al, "Paleogeographic and paleotectonic setting of Laramide sedimentary basins in the central Rocky Mountain region," *Geological Society of America Bulletin*, vol. 100, pp. 1023–1039, 1988.

[84] P. Bird, "Kinematic history of the Laramide orogeny in latitudes 35°-49°N, Western United States," *Tectonics*, vol. 17, no. 5, pp. 780–801, 1998.

[85] P. DeCelles and J. Coogan, "Regional structure and kinematic history of the Sevier fold-and-thrust belt, central Utah," *Geological Society of America Bulletin*, vol. 118, nos. 7–8, pp. 841–864, 2006.

[86] C. J. Busby and K. Putirka, "Miocene evolution of the western edge of the Nevadaplano in the central and northern Sierra Nevada: Palaeocanyons, magmatism, and structure," *International Geology Review*, vol. 51, nos. 7–8, pp. 670–701, 2009.

[87] E. J. Cassel, M. E. Smith, and B. R. Jicha, "The impact of slab rollback on earth's surface: Uplift and extension in the Hinterland of the North American Cordillera," *Geophysical Research Letters*, vol. 45, no. 20, 2018.

[88] L. F. Hintze, "Geologic history of Utah," *Brigham Young University Geology Studies, Special Publication*, vol. 7, pp. 40–102, 1988.

[89] G. J. Axen, B. P. Wernicke, M. J. Skelly, and W. J. Taylor, "Mesozoic and Cenozoic tectonics of the Sevier thrust belt in the Virgin river valley area, Southern Nevada," in *Basin and Range extensional tectonics near the latitude of Las Vegas*, B.P. Wernicke, Ed., 176:pp. 123–154, Geological Society of America Memoir, Nevada, 1990.

[90] M. E. Stewart, W. J. Taylor, P. A. Pearthree, B. J. Solomon, and H. A. Hurlow, "Neotectonics, fault segmentation, and seismic hazards along the Hurricane fault in Utah and Arizona: An overview of environmental factors in an actively extending region," *Brigham Young University Geology Studies*, 235–260, 1997.

[91] M. E. Stewart, W. J. Taylor, P. A. Pearthree, B. J. Solomon, and H. A. Hurlow, "Field guide to neotectonics, fault segmentation, and seismic hazards along the Hurricane fault in southwestern Utah and Northwestern Arizona," *Brigham Young University Geology Studies*, 261–273, 1997.

[92] W. Lund, M. Hozik, and S. Hatfield, *Paleoseismic Investigation and Long-Term Slip History of the Hurricane Fault in Southwestern Utah, Paleoseismology of Utah, v. 14, Special Study 119*, Utah Geological Survey, Salt Lake City, 2007.

[93] H. D. Stenner, W. R. Lund, P. A. Pearthree, and L. E. Benjamin, "Hurricane fault in northwestern Arizona and Southwestern Utah: Arizona geological survey," Open-File Report 99-8, 1999.

[94] W. J. Arabasz and D. R. Julander, "Geometry of seismically active faults and crustal deformation within the Basin and Range-Colorado Plateau transition in Utah," *Geological Society of America Special Paper*, vol. 208, pp. 43–74, 1986.

[95] S. D. Bowman and W. J. Arabaz, "Utah earthquakes (1850–2016) and Quaternary faults: Utah Geological Survey Map 277, scale 1:500,000," 2017.

[96] G. E. Christenson and S. J. Nava, "Earthquake hazards of Southwestern Utah," in *Engineering and Environmental Geology of Southwestern Utah: Utah Geological Association Publication 21*, K.M. Harty, Ed., pp. 123–138, 1992.

[97] G. E. Christenson, ed., "The September 2, 1992 Ml 5.8 St. George earthquake, Washington County, Utah," *Utah Geological Survey Circular*. Vol. 88, 1995.

[98] W. R. Lund, W. J. Taylor, and P. A. Pearthree, "Structural development and paleoseismicity of the Hurricane fault, Southwestern Utah and Northwestern Arizona," Field guide to geologic excursions in southwestern Utah and adjacent areas of Arizona and Nevada Open File Report 02-172. Edited by W. R. Lund, Geological Society of America Rocky Mountain Section Meeting, Cedar City, 2002.

[99] H. E. Gregory, "The geology and geography of the Paunsaugunt region Utah," *U.S. Geological Survey Professional Paper*, vol. 226, pp. 1–116, 1951.

[100] G. W. Jackson, "Tectonic geomorphology of the Toroweap fault, Western Grand Canyon, Arizona: Implications for transgression of faulting on the ColoradoPplateau: Arizona Geological Survey," Open-File Report 90-4, 1990.

[101] J.-E. Lundstern and M. D. Zoback, "Multiscale variations of the crustal stress field throughout North America," *Nature Communications*, vol. 11, no. 1, 2020.

[102] I. M. Schiefelbein and W. J. Taylor, "Fault development in the Utah transition zone and High Plateaus subprovince: Geological Society of America Abstracts with Programs," vol. 32, p. 194, 2000.

[103] R. L. Bruhn and D. Wu, "Fault structure and earthquake properties: EOS, transactions," *American Geophysical Union*, vol. 74, p. 63, 1993.

[104] J. N. Brune, "Precariously balanced rocks and ground-motion maps for Southern California," *Bulletin of the Seismological Society of America*, vol. 86, no. 1A, pp. 43–54, 1996.

[105] K. A. Sargent and B. C. Philpott, *Geologic Map of the Kanab Quadrangle, Kane County, Utah, and Mohave and Coconino Counties*, U.S. Geological Survey Map GQ-1603, Arizona, 1987.

[106] W. L. Stokes, "Geology of Utah, Utah Museum of Natural History," in *University of Utah and Utah Geological and Mineral Survey Department of Natural Resources*, p. 280, 1988.

[107] S. T. Nelson and D. G. Tingey, "Time-transgressive and extension-related basaltic volcanism in Southwest Utah and vicinity," *Geological Society of America Bulletin*, vol. 109, no. 10, pp. 1249–1265, 1997.

[108] L. F. Hintze, "Geological history of Utah," *Brigham Young University Geology Studies*, vol. 20, p. 181, 1973.

[109] J. E. Marzolf, "This extended land: Geological journeys in the Southern Basin and Range: Field trip guidebook: Geological Society of America Cordilleran section meeting, UNLV Department of Geoscience Special Publication," in

Reconstruction of Late Triassic and Early and Middle Jurassic sedimentary basins: Southwestern Colorado Plateau to the Eastern Mojave Desert, D. Weide, and M.L. Faber, Eds., 2:pp. 177–200, 1988.

[110] P. D. Rowley, J. J. Anderson, and P. L. Williams, "A summary of Tertiary volcanic stratigraphy of the southwestern High Plateaus and adjacent Great Basin, Utah," *U.S.Geological Survey Bulletin*, B1–B20, 1975.

[111] W. J. Taylor, "Stratigraphic and lithologic analysis of the Claron Formation in southwestern Utah," *Utah Geological Survey Report*, vol. 93, p. 152, 1993.

[112] P. M. Goldstrand, "Tectonic development of Upper Cretaceous to Eocene strata of Southwestern Utah," *Geological Society of America Bulletin*, vol. 106, no. 1, pp. 145–154, 1994.

[113] E. I. Smith, A. Sánchez, D. Walker, and K. Wang, "Geochemistry of mafic magmas in the Hurricane volcanic field Utah: Implications for small- and large-scale chemical variability of the lithospheric mantle," *The Journal of Geology*, vol. 107, no. 4, pp. 433–448, 1999.

[114] R. F. Downing, E. I. Smith, T. L. Orndorff, T. L. Spell, and K. A. Zanetti, "Imaging of Colorado Plateau-Basin and Range transition zone using basalt geochemistry, geochronology, and geographic information system," in *The geologic Transition, High Plateaus to Great Basin - a symposium and field guide: Utah Geological Association Publication 30 and Pacific Section American Association of Petroleum Geologists Guidebook*, M.E. Erskine, J.E. Faulds, J.M. Bartley, and P.D. Rowley, Eds., 78th ed., pp. 127–155, 2001.

[115] A. D. Gibbs, "Balanced cross-section construction from seismic sections in areas of extensional tectonics," *Journal of Structural Geology*, vol. 5, no. 2, pp. 153–160, 1983.

[116] I. Davison, "Listric normal fault profiles: Calculation using bed-length balance and fault displacement," *Journal of Structural Geology*, vol. 8, no. 2, pp. 209–210, 1986.

[117] G. Williams and I. Vann, "The geometry of listric normal faults and deformation in their hangingwalls," *Journal of Structural Geology*, vol. 9, no. 7, pp. 789–795, 1987.

[118] B. Vendeville, "Mechanisms generating normal fault curvature: a review illustrated by physical models.," Edited by A. M. Roberts, G. Yielding, and B. Freeman *Geological Society, London, Special Publications*, vol. 56, no. 1, pp. 241–249, 1991.

[119] N. White and G. Yielding, "Calculating normal fault geometries at depth: Theory and examples," in *Geological Society, London, Special Publications*, A.M. Roberts, G. Yielding, and B. Freeman, Eds., 56:pp. 251–260, 1991.

[120] N. White, "A method for automatically determining normal fault geometry at depth," *Journal of Geophysical Research*, vol. 97, no. B2, pp. 1715–1733, 1992.

[121] H. G. Kerr and N. White, "Application of an inverse method for calculating three-dimensional fault geometries and slip vectors, Nun River field, Nigeria," *AAPG Bulletin*, vol. 80, pp. 432–444, 1996.

[122] T. Song and P. A. Cawood, "Effects of subsidiary faults on the geometric construction of listric normal fault systems," *AAPG Bulletin*, vol. 85, pp. 221–232, 2001.

[123] D. Durham and B. Surpless, "Assessing geothermal potential using 3D modeling and restoration of the Sevier fault system, Southern Utah," Trinity University Summer Research and Internship Symposium, Abstracts with Programs, Trinity University, San Antonio, Texas, 2023.

[124] K. F. Kuiper, A. Deino, F. J. Hilgen, W. Krijgsman, P. R. Renne, and J. R. Wijbrans, "Synchronizing rock clocks of earth history," *Science (New York, N.Y.)*, vol. 320, no. 5875, pp. 500–504, 2008.

[125] M. G. Best, E. H. McKee, and P. E. Damon, "Space-time-composition patterns of late Cenozoic mafic volcanism, Southwestern Utah and adjoining areas," *American Journal of Science*, vol. 280, no. 10, pp. 1035–1050, 1980.

[126] W. E. Bowers, "Geologic map of Bryce Canyon National Park and vicinity, Southwestern Utah," *United States Geological Survey Miscellaneous Investigations Series Map 2180, 1*, 24, 1991.

[127] G. H. Billingsley, "Geologic map of the Grandstand Quadrangle, northern Mohave County," Geological Survey Open-File Report 93-588, U.S, Arizona, 1993.

[128] C. M. Barton, D. J. Evans, C. R. Bristow, E. C. Freshney, and G. A. Kirby, "Reactivation of relay ramps and structural evolution of the Mere fault and Wardour Monocline, northern Wessex Basin," *Geological Magazine*, vol. 135, no. 3, pp. 383–395, 1998.

[129] D. Zampieri, "Segmentation and linkage of the Lessini Mountains normal faults, Southern Alps, Italy," *Tectonophysics*, vol. 319, no. 1, pp. 19–31, 2000.

[130] D. Commins, S. Gupta, and J. Cartwright, "Deformed streams reveal growth and linkage of a normal fault array in the Canyonlands Graben," *Geology*, vol. 33, no. 8, pp. 645–648, 2005.

[131] D. A. Ferrill, A. P. Morris, and K. J. Smart, "Stratigraphic control on extensional fault propagation folding: Big brushy Canyon Monocline, Sierra del Carmen, Texas.," Edited by S. J. Jolley, D. Barr, J. J. Walsh, and R. J. Knipe *Geological Society, London, Special Publications*, vol. 292, no. 1, pp. 203–217, 2007.

[132] D. Ferrill, A. Morris, R. McGinnis, K. Smart, and W. Ward, "Fault zone deformation and displacement partitioning in mechanically layered carbonates: the Hidden Valley fault, central Texas," *AAPG Bulletin*, vol. 95, no. 8, pp. 1383–1397, 2011.

[133] L. Maerten, "Variation in slip on intersecting normal faults-implications for paleostress inversion," *Journal of Geophysical Research*, vol. 105, no. B11, pp. 25553–25565, 2000.

[134] L. Maerten, D. Pollard, and F. Maerten, "Digital mapping of three-dimensional structures of the Chimney Rock fault system, central Utah," *Journal of Structural Geology*, vol. 23, no. 4, pp. 585–592, 2001.

[135] R. H. Sibson, "A note on fault reactivation," *Journal of Structural Geology*, vol. 7, no. 6, pp. 751–754, 1985.

[136] C. Collettini and R. H. Sibson, "Normal faults normal friction?," *Geology*, vol. 29, no. 10, pp. 927–930, 2001.

[137] C. Collettini, T. Tesei, M. Scuderi, B. Carpenter, and C. Viti, "Beyond Byerlee friction, weak faults and implications for slip behavior," *Earth and Planetary Science Letters*, vol. 519, pp. 245–263, 2019.

[138] S. G. Wesnousky, "Seismological and structural evolution of strike-slip faults," *Nature*, vol. 335, no. 6188, pp. 340–343, 1988.

[139] A. Sagy, E. Brodsky, and G. Axen, "Evolution of fault-surface roughness with slip," *Geology*, vol. 35, no. 3, pp. 283–286, 2007.

[140] R. Gawthorpe and M. Leeder, "Tectono-sedimentary evolution of active extensional basins," *Basin Research*, vol. 12, nos. 3–4, pp. 195–218, 2000.

[141] B. Trudgill, "Structural controls on drainage development in the Canyonlands Grabens of Southeast Utah," *AAPG Bulletin*, vol. 86, pp. 1095–1112, 2002.

[142] M. A. Grant and P. F. Bixley, *Geothermal Reservoir Engineering*. 2nd Edition, Academic Press, Burlington MA, 2011.

[143] R. H. Sibson, "Crustal stress, faulting and fluid flow.," Edited by J. Parnell *Geological Society, London, Special Publications*, vol. 78, no. 1, pp. 69–84, 1994.

[144] H. Sibson, "Structural permeability of fluid-driven fault-fracture meshes", *Journal of Structural Geology*, vol. 18, no. 8, pp. 1031–1042, 1996.

[145] D. L. Siler, J. E. Faulds, B. Mayhew, and D. D. McNamara, "Analysis of the favorability for geothermal fluid flow in 3D: Astor Pass geothermal prospect, Great Basin, Northwestern Nevada, USA," *Geothermics*, vol. 60, pp. 1–12, 2016.

[146] P. Cowie, "Fault tip displacement gradients and process zone dimensions," *Journal of Structural Geology*, vol. 20, pp. 983–997, 1998.

[147] G. P. Thelin and R. J. Pike, "Landforms of the Conterminous United States - A Digital shaded-relief portrayal: U.S.G.S," *Geologic Investigations Series*, vol. I, p. 2720, 1991.

[148] B. E. Surpless and C. McKeighan, "The role of dynamic fracture branching in the evolution of fracture networks: An outcrop study of the Jurassic Navajo Sandstone, Southern Utah," *Journal of Structural Geology*, vol. 161, 2022.

[149] W. B. Cashion, "Geology and fuel resources of the Green River Formation, southeastern Uinta Basin, Utah and Colorado: U.S," *Geological Survey Professional Paper*, vol. 548, p. 48, 1967.